STRUCTURAL BIOLOGY

Structural insights into the unexpected agonism of tetracyclic antidepressants at serotonin receptors 5-HT_{1e}R and 5-HT_{1F}R

Gregory Zilberg[1,2]†, Alexandra K. Parpounas[2]†, Audrey L. Warren[2]†, Bianca Fiorillo[2], Davide Provasi[2], Marta Filizola[2], Daniel Wacker[1,2,3]*

Serotonin [5-hydroxytryptamine (5-HT)] acts via 13 different receptors in humans. Of these receptor subtypes, all but 5-HT_{1e}R have confirmed roles in native tissue and are validated drug targets. Despite 5-HT_{1e}R's therapeutic potential and plausible druggability, the mechanisms of its activation remain elusive. To illuminate 5-HT_{1e}R's pharmacology in relation to the highly homologous 5-HT_{1F}R, we screened a library of aminergic receptor ligands at both receptors and observe 5-HT_{1e}R/5-HT_{1F}R agonism by multicyclic drugs described as pan-antagonists at 5-HT receptors. Potent agonism by tetracyclic antidepressants mianserin, setiptiline, and mirtazapine suggests a mechanism for their clinically observed antimigraine properties. Using cryo-EM and mutagenesis studies, we uncover and characterize unique agonist-like binding poses of mianserin and setiptiline at 5-HT_{1e}R distinct from similar drug scaffolds in inactive-state 5-HTR structures. Together with computational studies, our data suggest that these binding poses alongside receptor-specific allosteric coupling in 5-HT_{1e}R and 5-HT_{1F}R contribute to the agonist activity of these antidepressants.

INTRODUCTION

Serotonin [5-hydroxytryptamine (5-HT)] is a conserved neurotransmitter that coordinates the physiological parameters of diverse processes across organ systems ranging from memory, mood, and sleep to gastrointestinal motility and vasodilation (*1*, *2*). In humans, the effects of 5-HT are mediated by 13 5-HT receptors (5-HTRs), 12 of which are G protein–coupled receptors (GPCRs) whereas 5-HT_3Rs comprise a family of pentameric ligand-gated ion channels (*1*). Because of 5-HT's important role in human health and disease inside and outside the central nervous system, 5-HTRs are targeted by numerous medications and illicit drugs and thus represent major drug targets for many conditions (*3*). For instance, within the 5-HT_1R subfamily, 5-HT_{1A}R is targeted by antidepressants and anxiolytics such as buspirone and vilazodone, while 5-HT_{1B}R, 5-HT_{1D}R, and, to a lesser extent, 5-HT_{1F}R are targeted by antimigraine triptan medications such as sumatriptan and frovatriptan (*4*, *5*). In notable contrast, there are only limited reports on the potential (patho) physiological role of the understudied receptor 5-HT_{1e}R, including select studies on its potential to treat cancer or exploit its proposed neuroprotective role (*6*, *7*). The International Union of Basic and Clinical Pharmacology considers 5-HT_{1e}R the sole orphan receptor among 5-HTRs as indicated with a lowercase appellation (*1*). This is the result of a lack of (i) 5-HT_{1e}R–selective compounds, (ii) studies on the receptor's pharmacology and molecular mechanisms, and, critically, (iii) a genetically accessible rodent orthologue for knockout experiments (*8*–*10*). For instance, the allegedly 5-HT_{1e}R–selective high-affinity agonist BRL-54443 (*8*) exhibits equal or superior potency at the highly homologous receptor 5-HT_{1F}R (*9*). Like 5-HT_{1e}R, 5-HT_{1F}R is also an understudied 5-HTR. However, 5-HT_{1F}R has been implicated in migraine pathophysiology, and lasmiditan (Reyvow), a 5-HT_{1F}R–selective drug, has recently been approved for treating migraines (*11*). 5-HT_{1e}R and 5-HT_{1F}R are routinely left out of off-target testing in most publications focusing on 5-HTRs; 5-HT_{1F}R in particular is not routinely tested by the National Institutes of Health (NIH) psychoactive drug screening program (PDSP) in their standard binding and cyclic adenosine 3′,5′-monophosphate (cAMP) inhibition panels (*12*). As a result, potential activities of known serotonergic drugs at these enigmatic receptors remain largely unknown, although many of these are "pan-aminergic" drugs that are known to have high affinity at multiple 5-HTR subtypes. While this oversight contributes to our poor understanding of 5-HT_{1e}R and 5-HT_{1F}R's pharmacological and molecular mechanisms, examining the activity of serotonergic drugs may uncover physiological (side) effects of drugs mediated by these receptors. Moreover, such activity could potentially be harnessed to explore pharmacophores that yield receptor-selective probes, such as first in class 5-HT_{1e}R–selective tool compounds with which to explore previous suggestions of 5-HT_{1e}R as a viable pharmacological target in the treatment of certain types of cancers (*13*, *14*).

To address these gaps in our molecular understanding of 5-HT_{1e}R and 5-HT_{1F}R pharmacology and function, we herein combine pharmacological assays, cryo–electron microscopy (cryo-EM) structure determination, structure-activity relationship (SAR) studies, as well as computer simulations. Specifically, screening a focused library of aminergic compounds and drugs against both receptors reveals potent agonist activity by multiple compounds, including the multicyclic prescription drugs mianserin and pimethixene. We subsequently determined structures of 5-HT_{1e}R signaling complexes activated by the antidepressants mianserin and setiptiline and performed molecular dynamic (MD) simulations of these structures embedded in an explicit lipid-water environment, as well as in vitro pharmacological assays. Our data reveal key insights into the binding of nontryptamine agonists at 5-HT_{1e}R and 5-HT_{1F}R, provide

[1]Department of Neuroscience, Icahn School of Medicine at Mount Sinai, New York, NY 10029, USA. [2]Department of Pharmacological Sciences, Icahn School of Medicine at Mount Sinai, New York, NY 10029, USA. [3]Department of Genetics and Genomic Sciences, Icahn School of Medicine at Mount Sinai, New York, NY 10029, USA.
*Corresponding author. Email: daniel.wacker@mssm.edu
†These authors contributed equally to this work.

insights into clinically reported side effects of mianserin and its analogs, and offer hints at how these supposedly pan-antagonistic compounds activate these enigmatic receptors.

RESULTS

Curated library screening uncovers activity of aminergic medications and research chemicals at serotonin receptors 5-HT$_{1e}$R and 5-HT$_{1F}$R

Functional efficacies of drugs known to interact nonselectively with monoaminergic receptors are poorly characterized at 5-HT$_{1e}$R and 5-HT$_{1F}$R relative to other 5-HTRs. A closer examination of these interactions could provide additional insight into their physiological roles and potentially explain drug side effects.

We thus set out to characterize the effects of selected medications and research chemicals for aminergic GPCRs at both receptors to define their molecular properties and potentially obtain novel pharmacological leads for the development of future receptor-selective probes (Fig. 1 and fig. S1). Like the other members of the 5-HT$_1$R family, 5-HT$_{1e}$R and 5-HT$_{1F}$R activation stimulates inhibitory G proteins such as G_{i1-3}, G_o, and G_z, which inhibit adenylyl cyclase, thereby lowering cellular cAMP levels. Likewise, 5-HT$_{1e}$R is capable

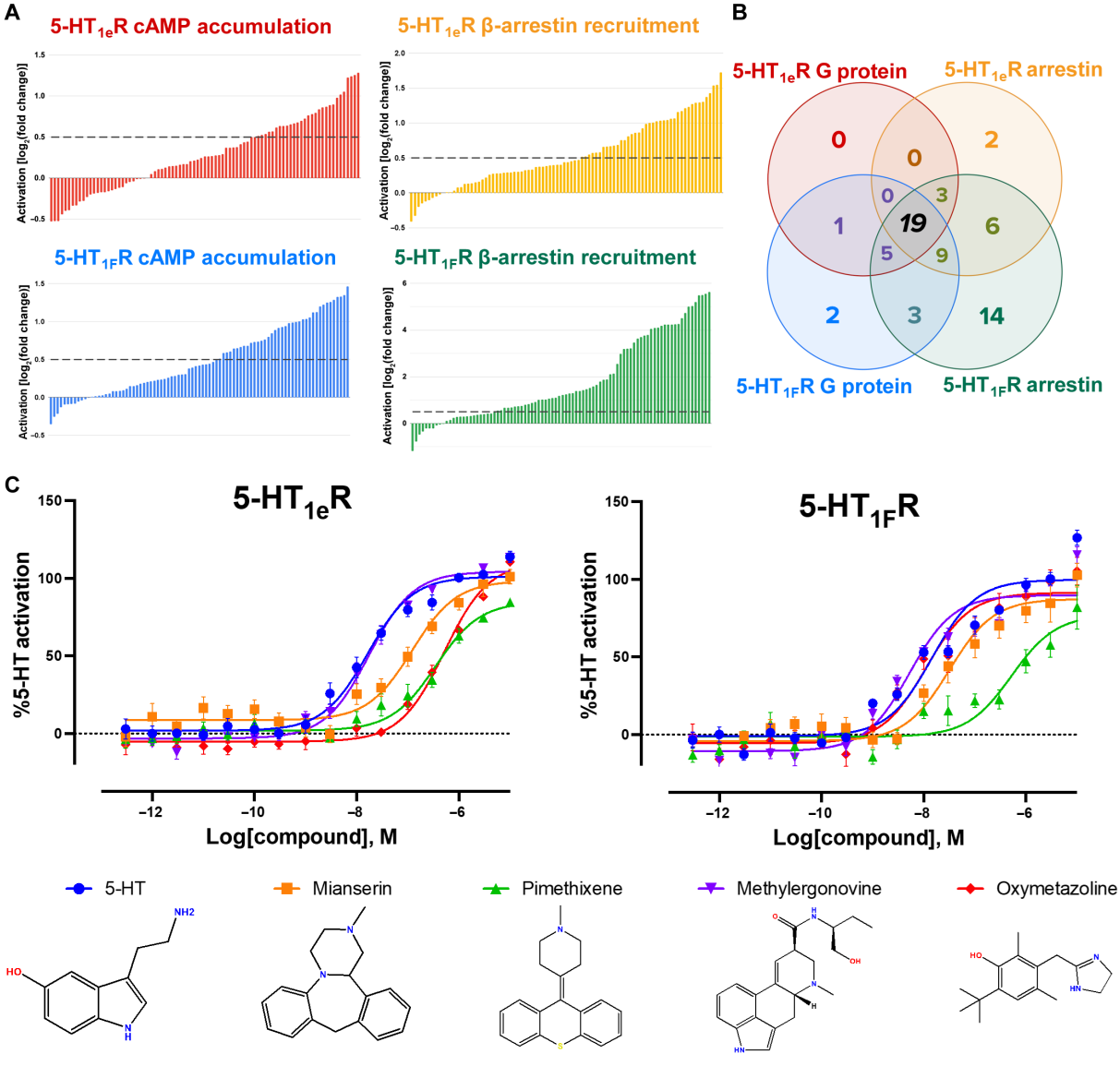

Fig. 1. A curated screen of aminergic receptor ligands reveals 5-HT$_{1e}$R and 5-HT$_{1F}$R agonism by chemically diverse drugs and research chemicals. (**A**) Activation of 5-HT$_{1e}$R and 5-HT$_{1F}$R as measured by cAMP accumulation and β-arrestin2 recruitment performed in human embryonic kidney (HEK) 293T cells. Experiments were performed in quadruplicate using 10 μM ligand concentration, and data are shown as $\log_2$ fold change with compounds considered active when above 0.5 (dashed line). β-Arrestin2 recruitment data were normalized against DMSO, and cAMP accumulation data were normalized against effects in cells not transfected with receptor. For details, see table S1. (**B**) Venn diagram showing the number of compounds active in a single or multiple screens. (**C**) Two-dimensional (2D) chemical structures and respective concentration response curves in 5-HT$_{1e}$R– or 5-HT$_{1F}$R–mediated G_{i1} protein dissociation in HEK293T cells. Experiments were performed in triplicate, and mean ± SEM from at least two ($n = 2$) independent experiments were averaged and normalized to 5-HT's response. For details, see table S2.

of recruiting arrestin to terminate G protein signaling or engage in noncanonical signaling (*14*). Thus, to test potential agonist activity of aminergic drugs at 5-HT_{1e}R and 5-HT_{1F}R, we measured receptor-mediated reduction in cellular cAMP using the GloSensor biosensor. This reporter produces luminescence in a cAMP concentration–dependent manner, allowing us to determine 5-HT_{1e}R activation as a function of reduction in cAMP levels (fig. S1) (*15*). We also measured receptor-mediated β-arrestin2 recruitment (*1*, *16*) via the PRESTO-Tango assay (*17*, *18*). In this assay, arrestin recruitment liberates a transcriptional activator from the receptor construct, thereby producing luciferase as a function of 5-HT_{1e}R activation (fig. S2). We validated both assays using 5-HT before assaying a panel of 87 selected aminergic receptor ligands, including endogenous neurotransmitters such as 5-HT and histamine, research chemicals, and clinically used drugs at 10 μM concentration (Fig. 1A and table S1). We herein found a high number of agonist activities, which we defined as an increase of at least fourfold (log_2 fold change of 2) of luminescent signal over dimethyl sulfoxide (DMSO)–treated controls: Sixty-four compounds showed agonist activity in at least one pathway of either 5-HT_{1e}R or 5-HT_{1F}R (Fig. 1, A and B, and table S1).

Of the compounds screened, 36 ligands activated both receptors across at least three screens (Fig. 1B), including the canonical agonist 5-HT, the 5-HT_{1e}R/5-HT_{1F}R–selective agonist BRL-54443, and 2-Br-LSD in agreement with a recent report (*19*). Twenty-one of these 36 compounds showed sub–10 μM affinity at either 5-HT_{1e}R, 5-HT_{1F}R, or both, in prior studies (*12*, *19*), while no activity at the tested receptors has been reported for the remaining 15 compounds (table S1; see the "Screening analysis" section in Materials and Methods for how active compounds were determined). In addition, we observed that three compounds, the 5-HT_{1A}R partial agonists buspirone and ipsapirone, and the antipsychotic raclopride showed substantial activity in both 5-HT_{1F}R screens without notable activity in the corresponding 5-HT_{1e}R assays (Fig. 1B and table S1).

To validate our results from the large-scale screens and determine potencies and efficacies of a subset of these compounds, we performed concentration-response experiments using an orthogonal bioluminescent resonance energy transfer (BRET) G protein activation assay (*20*). Specifically, reduced BRET efficiency between RLuc-tagged Gα subunits and enhanced green fluorescent protein–tagged Gγ/Gβ subunits serves as a marker of 5-HT_{1e}R activating (and thus dissociating) heterotrimeric G proteins (fig. S3). Of the compounds tested, we report nanomolar potencies for methylergonovine [5-HT_{1e}R median effective concentration (EC_{50}) = 17.0 nM, 5-HT_{1F}R EC_{50} = 5.2 nM], oxymetazoline (5-HT_{1e}R EC_{50} = 516.4 nM, 5-HT_{1F}R EC_{50} = 11.3 nM), pimethixene (5-HT_{1e}R EC_{50} = 353.1 nM, 5-HT_{1F}R EC_{50} = 456.0 nM), and mianserin (5-HT_{1e}R EC_{50} = 123.3 nM, 5-HT_{1F}R EC_{50} = 47.5 nM), while all other tested compounds exhibited weak-to-moderate micromolar potency agonism at both receptors (Fig. 1C and see table S2 for SEM).

Studies previously reported 5-HT_{1e}R and 5-HT_{1F}R agonism of methylergonovine (Methergine, a second-line uterotonic and potential antimigraine agent), while agonism of oxymetazoline (Afrin, a topical decongestant and alpha-adrenergic receptor agonist) was only described for 5-HT_{1F}R, 5-HT_{1A}R, 5-HT_{1B}R, and 5-HT_{1D}R but not 5-HT_{1e}R (*21*, *22*). By contrast, the potent agonism of pimethixene (Muricalm, an antihistamine and anticholinergic) and mianserin (Tolvon, a noradrenergic and specific serotonin antidepressant) was unexpected due to their reported antagonism for several GPCRs. Specifically, pimethixene is an antagonist at histamine, serotonin, and muscarinic acetylcholine receptors (*23*, *24*), and mianserin is an antagonist at alpha-adrenergic and 5-HT_2 receptors (*25*, *26*), although weak partial agonism (EC_{50} = 530 nM) has been reported at the kappa opioid receptor (*27*).

Functional characterization supports unexpected 5-HT_{1e}R and 5-HT_{1F}R agonism of tetracyclic antidepressants and structurally related drugs

Since mianserin's high potency and agonism were particularly unexpected, we sought confirmation of its atypical activity at 5-HT_{1e}R and 5-HT_{1F}R. Several studies describe mianserin as a pan-aminergic, panserotonergic, or nonselective 5-HT_2R and adrenergic α_2R antagonist (*28*–*30*). We therefore decided to investigate the possible extension of this agonism to other similar human 5-HTRs using the previously described β-arrestin2 recruitment assay (fig. S4). In this assay, mianserin potently activated 5-HT_{1e}R (EC_{50} = 67 nM) with full efficacy, while it produced markedly weaker partial agonism at 5-HT_{1F}R (EC_{50} = 667 nM, E_{max} = 24%) and 5-HT_{1D}R (EC_{50} = 371 nM, E_{max} = 25%). In contrast, no noticeable agonism was observed at any of the other 5-HTRs, with potential inverse agonism at 5-HT_{2A}R and 5-HT_{2B}R at high concentrations. Likewise, pimethixene-mediated arrestin recruitment at these receptors showed full agonism at 5-HT_{1e}R (EC_{50} = 453 nM), but no noticeable activity at the other receptors tested apart from high concentrations at 5-HT_{1A}R (see fig. S4). Together, we find that mianserin and pimethixene not only display selective agonism for 5-HT_{1e}R and 5-HT_{1F}R, but they also display distinct pharmacological activities at the two receptors. Specifically, both drugs appear to be balanced agonists in different pathways downstream of 5-HT_{1e}R, but they are biased toward G protein pathways at 5-HT_{1F}R.

Given the atypical receptor agonism of the multicyclic drugs mianserin and pimethixene, scaffolds that typically antagonize aminergic GPCRs (*31*), we next systematically investigated the 5-HT_{1e}R and 5-HT_{1F}R activity of other compounds and clinically used medications with related scaffolds (Fig. 2). Among the tested compounds, several drugs including the muscle relaxant cyclobenzaprine (Amrix), as well as the antipsychotics chlorpromazine (Thorazine) and clozapine (Clozaril), display nanomolar potency at either 5-HT_{1e}R or 5-HT_{1F}R, albeit with distinct selectivities and efficacies. It should be noted that binding affinities, but not functional efficacies, of clozapine and chlorpromazine have been previously reported for 5-HT_{1e}R and 5-HT_{1F}R (*32*).

These findings show that even multicyclic scaffolds distinct from that of mianserin can activate 5-HT_{1e}R and 5-HT_{1F}R. Using the G protein BRET assay, we subsequently determined that setiptiline and mirtazapine, both tetracyclic antidepressants (TeCAs), and closely related structural analogs of mianserin exhibit the most potent and efficacious activity among the multicyclic drugs tested. Specifically, we find that setiptiline is a potent full agonist at both 5-HT_{1e}R (EC_{50} = 171.0 nM) and 5-HT_{1F}R (EC_{50} = 64.6 nM), whereas mirtazapine shows reduced potency at 5-HT_{1e}R (EC_{50} = 1.04 μM) relative to 5-HT_{1F}R (EC_{50} = 235.5 nM) (Fig. 2). Together, these findings uncover unique aspects of 5-HT_{1e}R and 5-HT_{1F}R's molecular pharmacology and illuminate previously underexplored facets of the polypharmacology of mianserin and related prescription drugs.

Cryo-EM studies of 5-HT_{1e}R–$G\alpha_{i1}$–$G\beta_1$–$G\gamma_2$ complexes illuminate structural features of 5-HT_{1e}R bound by TeCAs

Despite the clinical use of mianserin and related TeCAs, little is known about how they bind on-target receptors, let alone how

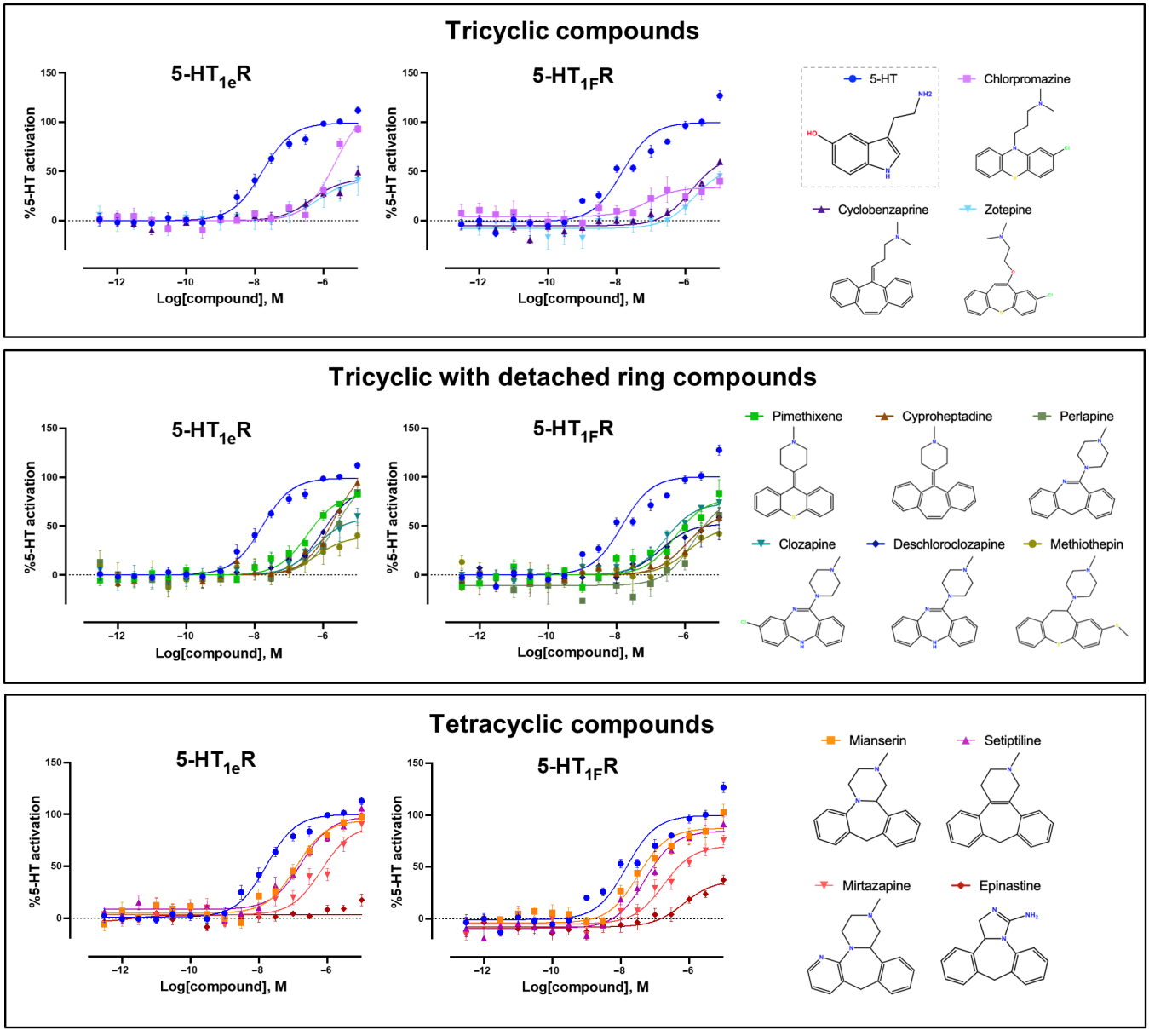

Fig. 2. Activities of multicyclic drugs at 5-HT$_{1e}$R and 5-HT$_{1F}$R. 2D chemical structures and respective concentration response curves in 5-HT$_{1e}$R– or 5-HT$_{1F}$R–mediated G_{i1} protein dissociation in HEK293T cells are shown. Experiments were performed in triplicate, and mean ± SEM from at least two (n = 2) independent experiments were averaged and normalized to 5-HT's response. For details, see table S2.

they activate 5-HT$_{1e}$R and 5-HT$_{1F}$R. To elucidate the molecular basis of these mechanisms, we next determined cryo-EM structures of mianserin- and setiptiline-bound 5-HT$_{1e}$R–G protein signaling complexes. This was done largely following previously published methodology (see Materials and Methods) (Fig. 3A, figs. S5 and S6, and table S3) (*33*). Briefly, 5-HT$_{1e}$R containing a L111$^{3.41}$W mutation [superscripts denote Ballesteros-Weinstein numbering (*34*)] and $G\alpha_{i1}\beta_1\gamma_2$ (G_{i1}) were separately expressed (*35*), subsequently combined in the presence of agonist, and complexes were isolated by gel filtration chromatography. Peak fractions were concentrated and frozen on grids and subsequently imaged and processed to obtain high-resolution cryo-EM reconstructions. Mianserin- and setiptiline-bound 5-HT$_{1e}$R–G_{i1} complex structures were determined at global resolutions of 3.30 and 3.32 Å, respectively, with local resolutions of ~3.0 and ~3.2 Å for the ligand binding pockets (figs. S5 and S6 and table S3). At these resolutions, we were able to unambiguously identify residue conformers within the ligand-binding pocket and elucidate mianserin and setiptiline's binding poses and drug-receptor interactions (figs. S5B and S6B). Our structures further enabled modeling of additional residues F159$^{4.62}$ and W160$^{4.63}$ in transmembrane helix 4 (TM4), residues P170-Q172 in ECL2 and residues Y213$^{5.69}$-R216$^{5.72}$ at the cytoplasmic end of TM5 not observed in the previous structure of BRL-54443–bound 5-HT$_{1e}$R–G_{i1} (fig. S7) (*33*).

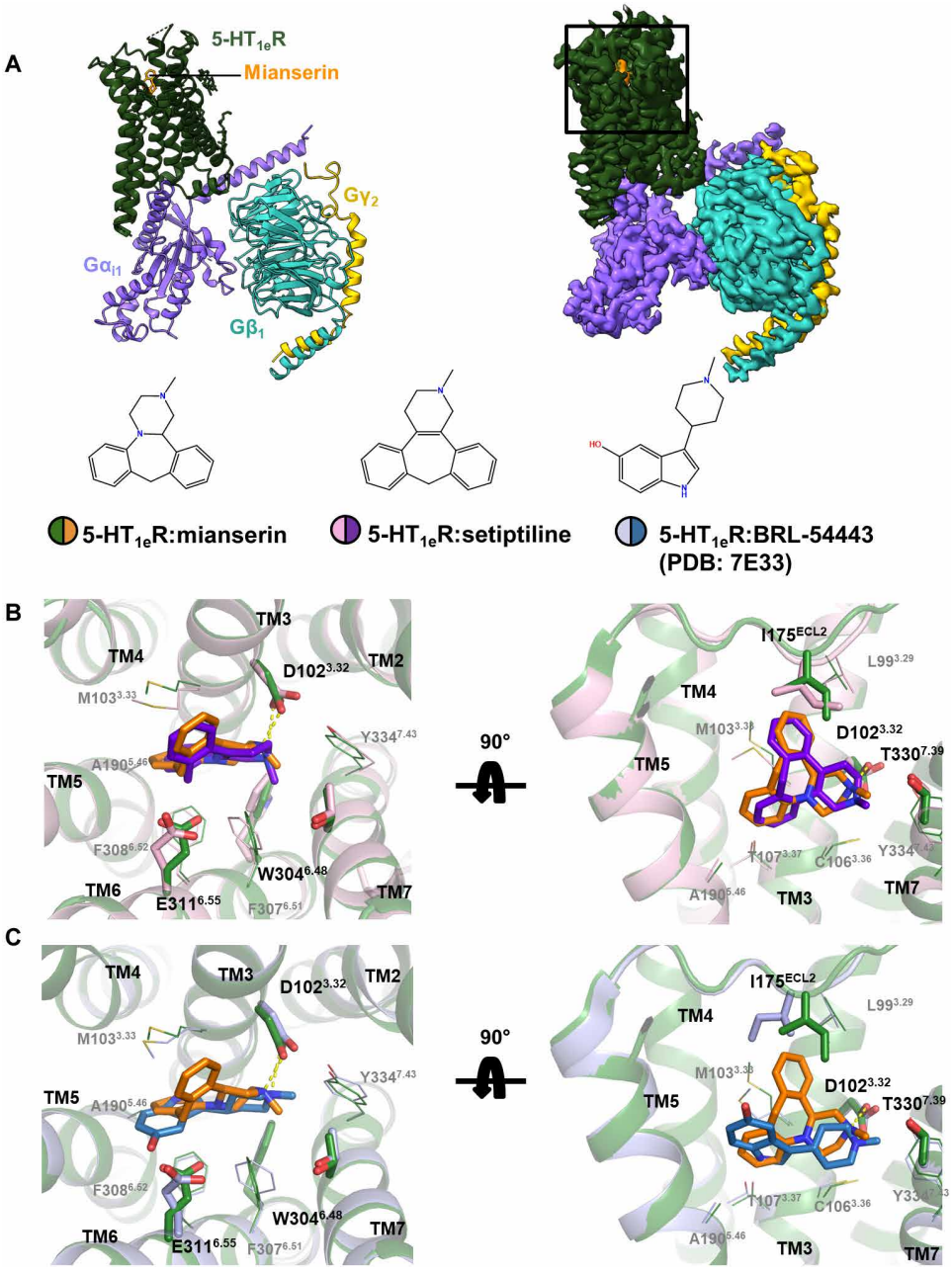

Fig. 3. Cryo-EM structure determination of mianserin- and setiptiline-bound 5-HT$_{1e}$R–Gα_{i1}–Gβ_1–Gγ_2 complex. (**A**) 2D chemical structures of structurally characterized 5-HT$_{1e}$R agonists (bottom) and overall structural model (left) and cryo-EM map (right) of mianserin-bound 5-HT$_{1e}$R–Gα_{i1}–Gβ_1–Gγ_2 complex. Mianserin, 5-HT$_{1e}$R, Gα_{i1}, Gβ_1, and Gγ_2 are colored in orange, green, violet, teal, and yellow. (**B**) Superposition of orthosteric ligand binding pockets of mianserin- and setiptiline-bound 5-HT$_{1e}$R. (**C**) Superposition of orthosteric ligand binding pockets of mianserin- and BRL-54443–bound 5-HT$_{1e}$R. Key side chains and drugs are shown as sticks, and a conserved salt bridge between drugs and D3.32 is shown as yellow dashed lines. Mianserin–5-HT$_{1e}$R complex is colored in orange and green, setiptiline–5-HT$_{1e}$R complex is colored in purple and pink, and BRL-54443–5-HT$_{1e}$R complex [Protein Data Bank (PDB): 7E33] is colored in dark blue and light blue.

Overall, our structures are similar to the previously published BRL-54443–bound 5-HT$_{1e}$R–G$_{i1}$ structure (*33*). Comparison of the mianserin- and setiptiline-bound complexes with that of the BRL-54443–bound complex yielded minimal global differences, with overall root mean square deviations (RMSDs) of 0.66 and 0.63 Å, respectively (Fig. 3, B and C). The structures exhibit previously described hallmarks of activated GPCRs. For instance, the cytoplasmic tip of TM6 is moved outward relative to inactive-state structures (discussed below) to accommodate the C-terminal α-helical domain of Gα_{i1}. These changes likely originate from a torsion motion around F251$^{6.44}$ of the P$^{5.50}$-I$^{3.40}$-F$^{6.44}$ motif that allosterically links ligand- and transducer-binding pockets (*36*). Compared to the previous structure (*33*), we observe additional densities for residues 158 to 160 at the extracellular side of TM4, the backbone of side chains 170 and

171 at the end of extracellular loop 2 (ECL2), and TM5 residues 213 to 217 (fig. S7, A and B). However, our structures lack density for the TM6 segment corresponding to residues 282 to 285. These minor differences do not appear to account for pharmacological differences between mianserin-/setiptiline- and BRL-54443–mediated activation and likely reflect minor differences in sample and grid preparation. In contrast to the previous 5-HT_{1e}R structure, we identify several densities corresponding to membrane components. For instance, we observe two cholesterols that are bound near the intracellular junction of TM2, TM3, and TM4 (fig. S7C). In addition, a cholesterol-like density appears to bind within the crevice formed by TM3, TM4, and TM5, specifically forming an interaction with conserved Arg204$^{5.60}$ (fig. S7D). Last, four hydrophobic densities are found on the interface formed by TMs 1, 6, and 7, including one appearing to interact with Leu342$^{7.51}$ and one sitting in an extracellular pocket formed by Ile25$^{1.35}$ and Phe328$^{7.37}$ (fig. S7E).

Structural, computational, and functional studies elucidate the unique binding pose of TeCAs at 5-HT_{1e}R

Within the 5-HT_{1e}R ligand binding pocket, mianserin and setiptiline exhibit similar topologies, adopting an open C-shaped bend across their tricyclic moieties and forming a conserved salt bridge between a tertiary amine in their fourth ring and D102$^{3.32}$ (Fig. 3) (*37*). The piperazine ring of mianserin (analogously the tetrahydropyridine ring of setiptiline) resides near the conserved residues F307$^{6.51}$ and Y334$^{7.43}$, which form one end of the orthosteric binding pocket. These interactions position the tricyclic moiety perpendicularly to the membrane between TM3, TM5, and TM6 (Fig. 3B). Both compounds appear to contact similar orthosteric binding pocket residues (within 4 Å), forming mostly hydrophobic interactions with L99$^{3.29}$, M103$^{3.33}$, C106$^{3.36}$, T107$^{3.37}$, I175^{ECL2}, A190$^{5.46}$, W304$^{6.48}$, F308$^{6.52}$, E311$^{6.55}$, and T330$^{7.39}$ (Fig. 3B).

The majority of binding pocket residues adopt similar conformations in the structures of TeCA-bound and BRL-54443–bound 5-HT_{1e}R (Fig. 3, B and C) (*33*). However, there were notable differences. The tricyclic moieties of mianserin and setiptiline assume a unique binding pose that places part of their scaffolds closer to the extracellular space, where they occupy a site that has frequently been characterized as an extended binding pocket in other aminergic receptors (*38*). There, both drugs induce a displacement and rotation of I175^{ECL2} away from TM3 relative to BRL-54443 (Fig. 3C). In the setiptiline-bound structure, the electrostatic potential maps even suggest that I175^{ECL2} forms a more extended interface with the tricyclic moiety compared to that observed for mianserin (figs. S5B and S6B). Furthermore, we observe a conformational change of E311$^{6.55}$ in the mianserin-bound but not the setiptiline-bound structure (Fig. 3B and figs. S5 and S6). To further investigate these subtle structural differences between mianserin- and setiptiline-bound 5-HT_{1e}R binding pockets and validate our structural models, we conducted both computational and mutational analyses.

To assess the stability of the binding modes of mianserin and setiptiline inferred by the density maps and uncover potential drug-related differences, we first performed four MD simulation replicas for a total of 1 μs for each ligand-receptor system and investigated ligand and receptor conformational flexibilities in an explicit lipid-water environment (see Materials and Methods for details) (Fig. 4, A and B). Both the receptor and ligands did not change significantly during the MD simulations as shown by their very low heavy-atom RMSD values [an average of 1.75 and 1.45 Å for mianserin and setiptiline, respectively, and an average of 1.69 and 1.49 Å for the receptor's backbone in complex with mianserin and setiptiline, respectively (fig. S8)]. A structural interaction fingerprint (SIFt) analysis (Fig. 4B) of the simulation trajectories confirmed that both mianserin and setiptiline maintain similar binding modes in the 5-HT_{1e}R orthosteric binding pocket during simulations through similar interactions with receptor residues. Specifically, the tricyclic moiety in both mianserin and setiptiline interacted with probabilities larger than 60% with L99$^{3.29}$, M103$^{3.33}$, I175^{ECL2}, A190$^{5.46}$, F308$^{6.52}$, and E311$^{6.55}$, whereas the methylpiperazine group of both ligands formed apolar interactions with probabilities larger than 60% with C106$^{3.36}$ and T330$^{7.39}$ (Fig. 4B). The two ligands also formed a stable π-π stacking interaction with F308$^{6.52}$ via the benzyl group of the tricyclic scaffold, as well as a hydrogen bond and a salt bridge with the side chain of D102$^{3.32}$ via their piperazine nitrogen, which are typically present in aminergic GPCRs (*36*, *37*). The most notable difference between the two ligands was an interaction formed with a probability larger than 30% by mianserin, but not setiptiline, with residue H177^{ECL2}.

Guided by our structural and computational analyses, we next interrogated the contributions of pocket residues to the distinct binding poses of mianserin and setiptiline when compared to the 5-HT analog BRL-54443. To this end, we determined the activities of 5-HT, BRL-54443, mianserin, and setiptiline at wild-type and mutant 5-HT_{1e}R using G protein dissociation (Fig. 4C, fig. S9, and table S4) and arrestin recruitment assays (fig. S10 and table S5) as well as radioligand binding studies (figs. S11 and S12 and table S6).

We found that [^{3}H]5-HT saturated wild-type 5-HT_{1e}R with an equilibrium dissociation constant (K_D) of 1.2 nM, and mianserin, setiptiline, and mirtazapine displaced [^{3}H]5-HT with equilibrium inhibition constants (K_is) of 26.1, 29.3, and 269.2 nM, respectively (fig. S11 and table S6). These values are in broad agreement with their potency in functional experiments, although it should be noted that these affinities are 2.8- to 5.8-fold higher than their potency in G protein activation but only 1.1- to 2.3-fold higher than their potency in arrestin recruitment.

Mutation of most ligand binding pocket residues nonspecifically reduced the potency of agonist-mediated G protein dissociation (table S4). On the basis of our G protein activation data, an I175^{ECL2}A mutation reduced the potency of 5-HT relative to mianserin and setiptiline, while mutation to a bulkier phenylalanine only marginally affected potencies (Fig. 4C, fig. S9, and table S4). Notably, an I175^{ECL2}W mutation had little effect on the tryptamines 5-HT and BRL-54443 but notably increased the potencies of the TeCA ligands mianserin (7.5 nM) and setiptiline (15 nM) by over 10-fold (fig. S9 and table S4). In contrast, responses to 5-HT, BRL-54443, mianserin, and setiptiline are largely unaffected in our arrestin recruitment assay, but mirtazapine's potency increased over fivefold at I175^{ECL2}W (fig. S10 and table S5). In radioligand binding studies, we observed that I175^{ECL2}W decreased the affinity of [^{3}H]5-HT ~3.7-fold relative to wild type (fig. S11 and table S6), and BRL-54443's affinity even decreased by 13.5-fold relative to wild type. In comparison, all three TeCA ligands tested displayed marginal decreases in affinity (fig. S12 and table S6).

We next mutated T330$^{7.39}$ to a valine, as found in 5-HT_2 receptors, which reduced the G protein activation potency of all ligands tested. T330$^{7.39}$V reduced the efficacy of both mianserin (E_{max} = 64.4% of 5-HT) and setiptiline (E_{max} = 62.1% of 5-HT) (Fig. 4C, fig. S9, and table S4). When measuring arrestin recruitment, we did not observe

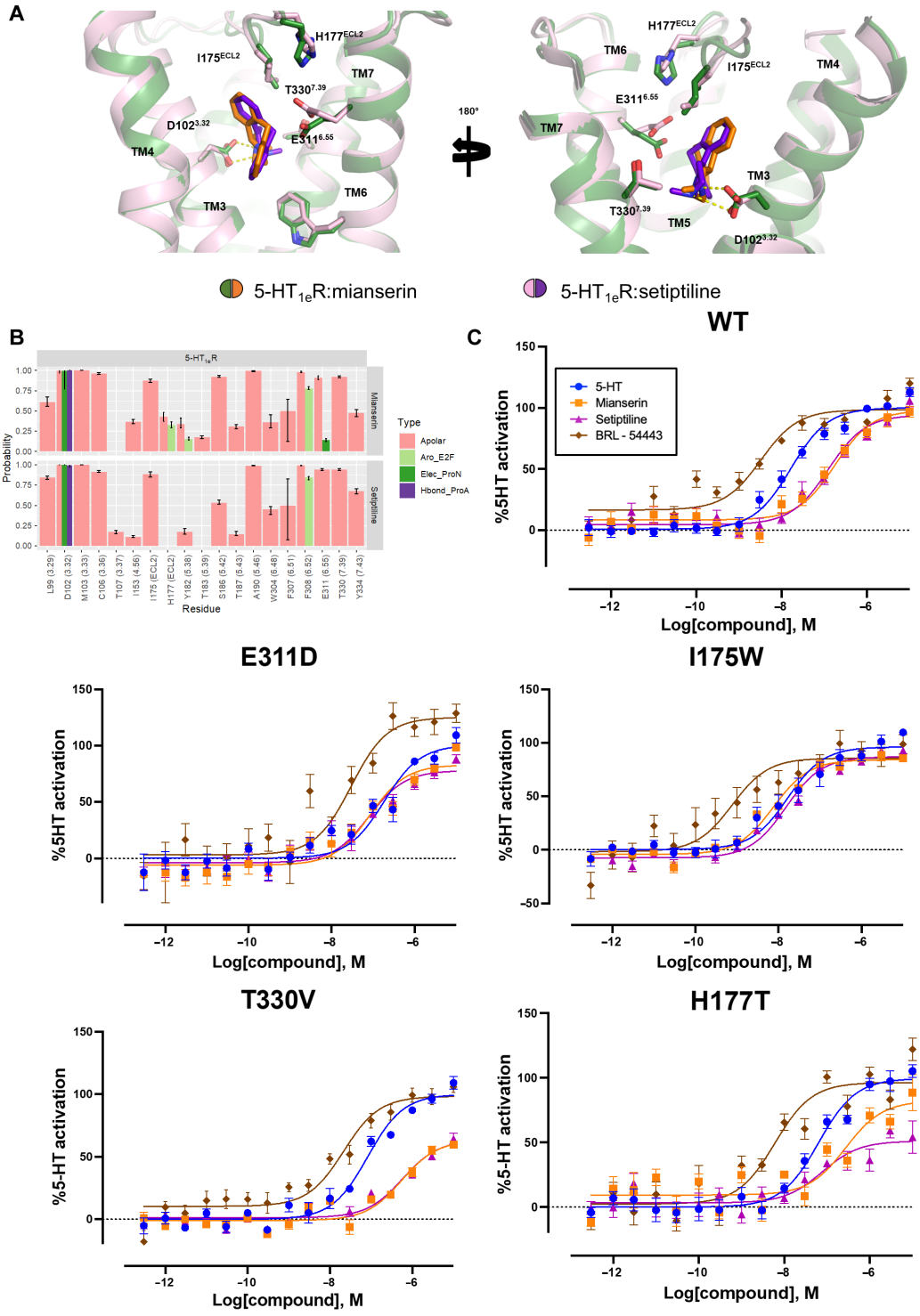

Fig. 4. Experimental and computational SAR studies of mianserin and setiptiline interactions with the 5-HT$_{1e}$R binding pocket. (**A**) Views of the mianserin- and setiptiline-bound 5-HT$_{1e}$R orthosteric pocket, with key residues interacting with drugs shown as sticks. Conserved salt bridges between drugs and D3.32 are shown as yellow dashed lines. Mianserin–5-HT$_{1e}$R complex is colored in orange and green, setiptiline–5-HT$_{1e}$R complex is colored in purple and pink. (**B**) SIFt analyses indicate probabilities of ligand-receptor interactions formed during four 250-ns MD simulations of the mianserin/setiptiline–5-HT$_{1e}$R systems. The four interaction types formed by the ligands with the protein backbone and side chains are carbon-carbon atomic interactions (Apolar, pink), edge-to-face aromatic (Aro_E2F, light green), hydrogen bond with the protein as the hydrogen bond acceptor (Hbond_ProA, purple), and electrostatic interaction with the protein negatively charged (Elec_ProN, light green). Only interactions with an average probability greater than 10% are displayed. (**C**) Concentration response experiments determining the activity of 5-HT, mianserin, setiptiline, and BRL-54443 at wild type (WT) and mutant 5-HT$_{1e}$R as measured by G$_{i1}$ BRET in HEK293T cells. Experiments were performed in triplicate, and mean ± SEM from at least two (n = 2) independent experiments were averaged and normalized to 5-HT's response. For details, see table S4.

this reduction in efficacy, although the potencies of mianserin and setiptiline were both considerably reduced (fig. S10 and table S5).

In agreement with the functional data, T330$^{7.39}$V decreased the affinity of [^{3}H]5-HT almost sevenfold relative to wild type. Likewise, the affinity of BRL-54443 decreased by 15.7-fold (K_i = 2.8 nM) (figs. S11 and S12 and table S6). However, TeCA affinities were disproportionately less affected. Setiptiline (3.3-fold, K_i = 96.4 nM) and mirtazapine (3.8-fold, K_i = 1,028.0 nM) had similar decreases in affinity, with mianserin (5.1-fold, K_i = 133.4 nM) affinity decreasing slightly more than the others.

Similarly, H177^{ECL2}, located next to E311$^{6.55}$, when mutated to phenylalanine or alanine, also reduced mianserin's efficacy in G protein activation (E_{max} = 60.5 and 62.2% of 5-HT, respectively). Notably, replacement with the polar residue threonine appeared to differentially affect the efficacies of setiptiline and mianserin (E_{max} = 51.2 and 78.3% of 5-HT, respectively), in line with the suggestion of different ligand-receptor interactions from our SIFt analysis. Mutation of H177^{ECL2}T also resulted in substantial decreases in the potencies of both mianserin and setiptiline in arrestin recruitment (fig. S10 and table S5). In line with the differential changes in efficacy in G protein activation, introduction of H177^{ECL2}T disproportionately decreased the affinity of setiptiline by 8.1-fold compared to the 4.5-fold reduced affinity of mianserin (fig. S12 and table S6).

E311$^{6.55}$ shows different conformations in the mianserin- and setiptiline-bound structures, and previous studies have highlighted the importance of interactions with residues at position 6.55 for ligand specificity (*39*). According to the SIFt analysis, E311$^{6.55}$ forms highly probable apolar interactions with both mianserin and setiptiline during simulation, but it forms an electrostatic interaction with mianserin only, albeit with a very low probability (Fig. 4B). We thus probed the role of E311$^{6.55}$ in ligand binding and/or receptor activation through substitution with glutamine, asparagine, or aspartate.

Ablating side chain charge through an E311$^{6.55}$Q mutation disproportionately reduced the potency of 5-HT (14.4-fold) compared to mianserin (1.9-fold) and setiptiline (3.1-fold) in G protein activation (fig. S9 and table S4). Reducing side chain length through an E311$^{6.55}$D mutation strongly reduced the potency of both tryptamine ligands by 13.9- to 19-fold, while it increased both mianserin's and setiptiline's potencies, effectively making them more potent than 5-HT (Fig. 4C and table S4). Conversely, in arrestin recruitment assays, the E311$^{6.55}$D mutation substantially reduced response to all ligands tested, with 5-HT, mianserin, or setiptiline yielding minimal response below 1 μM, while BRL-54443 was able to recruit arrestin with a roughly 200-fold decrease in potency (EC_{50} = 34.6 nM) compared to wild type (fig. S10 and table S5). Saturation binding of [^{3}H]5-HT to E311$^{6.55}$D (K_D = 9.0 nM) yielded low signal over background, precluding displacement assays (fig. S11 and table S6). Reducing the residue size and removing the charge through an E311$^{6.55}$N mutation resulted in markedly reduced potencies for 5-HT, setiptiline, and mianserin in G protein activation, where mianserin is notably the most potent of the three (fig. S9 and table S4).

Together, our comprehensive SAR experiments uncover and characterize how receptor residues differentially contribute to the activity of the TeCAs compared to 5-HT. These data further suggest that rather than any individual interaction, mianserin's and setiptiline's overall binding pose, including interactions with extended pocket residues, is likely responsible for their unexpected efficacious agonism at 5-HT$_{1e}$R (and likely 5-HT$_{1F}$R).

Structural comparisons yield molecular insights into the agonist activity of mianserin and setiptiline at 5-HT$_{1e}$R

In the absence of any unambiguous drug-receptor interactions responsible for the agonist efficacy of the tested TeCA medications at 5-HT$_{1e}$R, we turned to other approaches to analyze why these ligands are not antagonists, as with other 5-HTRs. We first compared our active state structures to the inactive-state structures of 5-HTRs bound to chemically related antagonists. Specifically, we used inactive-state structures of 5-HT$_{1B}$R bound to the multicyclic research chemical methiothepin and of 5-HT$_{2A}$R bound to the multicyclic antipsychotic zotepine for comparison (*40*, *41*). For ease of visualization, we show our analysis against only the mianserin-bound structure (Fig. 5A). As is the case for mianserin, both methiothepin and zotepine are anchored to their respective 5-HTRs via a conserved salt bridge with D$^{3.32}$ (*37*), and their multicyclic moieties adopt a kinked C-shaped conformation occupying the amphipathic orthosteric binding pocket. However, the binding pose of both antagonists is fundamentally different, with both methiothepin and zotepine binding in a mirrored orientation compared to mianserin. As a result, the tricyclic pharmacophore moieties of the antagonists are oriented closer toward TM6, which shows distinct positioning in active- and inactive-state structures (Fig. 5A). Since large-scale TM6 movements concomitant with conformational changes in the rotameric toggle switch W$^{6.48}$ are key elements for the transition from inactive to active state (*42*, *43*), differences in TM6 interactions could conceivably contribute to the divergent pharmacology of the different multicyclic compounds.

The multicyclic pharmacophores also extend deeper into their respective binding pockets than mianserin. Methiothepin and zotepine are bound 3.7 and 3.9 Å closer to the receptor core compared to mianserin's much shallower binding pose at 5-HT$_{1e}$R (Fig. 5A). We further observe that comparison with inactive-state structures of 5-HTRs bound to the chemically unrelated antagonist medications risperidone, aripiprazole, cariprazine, and ritanserin similarly feature deep protrusions of the antagonists into the binding pocket relative to mianserin (fig. S13). This further suggests that mianserin's shallow binding pose might facilitate activation-related conformational changes near the 7TM core of the receptor that are otherwise inhibited by the deeper binding pose of antagonists.

Since allosteric communication between ligand and G protein binding sites plays a key role in the divergent pharmacological activities of drugs at GPCRs (*44*), we wanted to understand whether there was a discernable mechanistic basis in downstream allosteric networks by which mianserin and setiptiline induced agonism of 5-HT$_{1e}$R. Toward this end, we analyzed the contributions of residues to the allosteric communication between the orthosteric ligand binding site and the receptor–G protein interface via transfer entropy analysis of our MD simulations (>3% flux) (Fig. 5B). Notably, most of these contributing residues were the same for the two simulated drug-bound 5-HT$_{1e}$R–G$_{i1}$ systems (Fig. 5B), suggesting an overall common allosteric mechanism induced by the two drugs throughout 5-HT$_{1e}$R. However, we do note differences for S238$^{6.27}$ and R287$^{6.31}$ at the receptor–G protein interface, as well as T107$^{3.37}$, I153$^{4.56}$, H177^{ECL2}, Y182$^{5.39}$, and F308$^{6.52}$ in the binding pocket. Some of the ligand-receptor interactions identified by the SIFt analysis (specifically, with residues C106$^{3.36}$, E311$^{6.55}$, T330$^{7.39}$, and Y334$^{7.43}$) do not appear to be involved in the allosteric coupling between the ligand binding pocket and the intracellular side of the

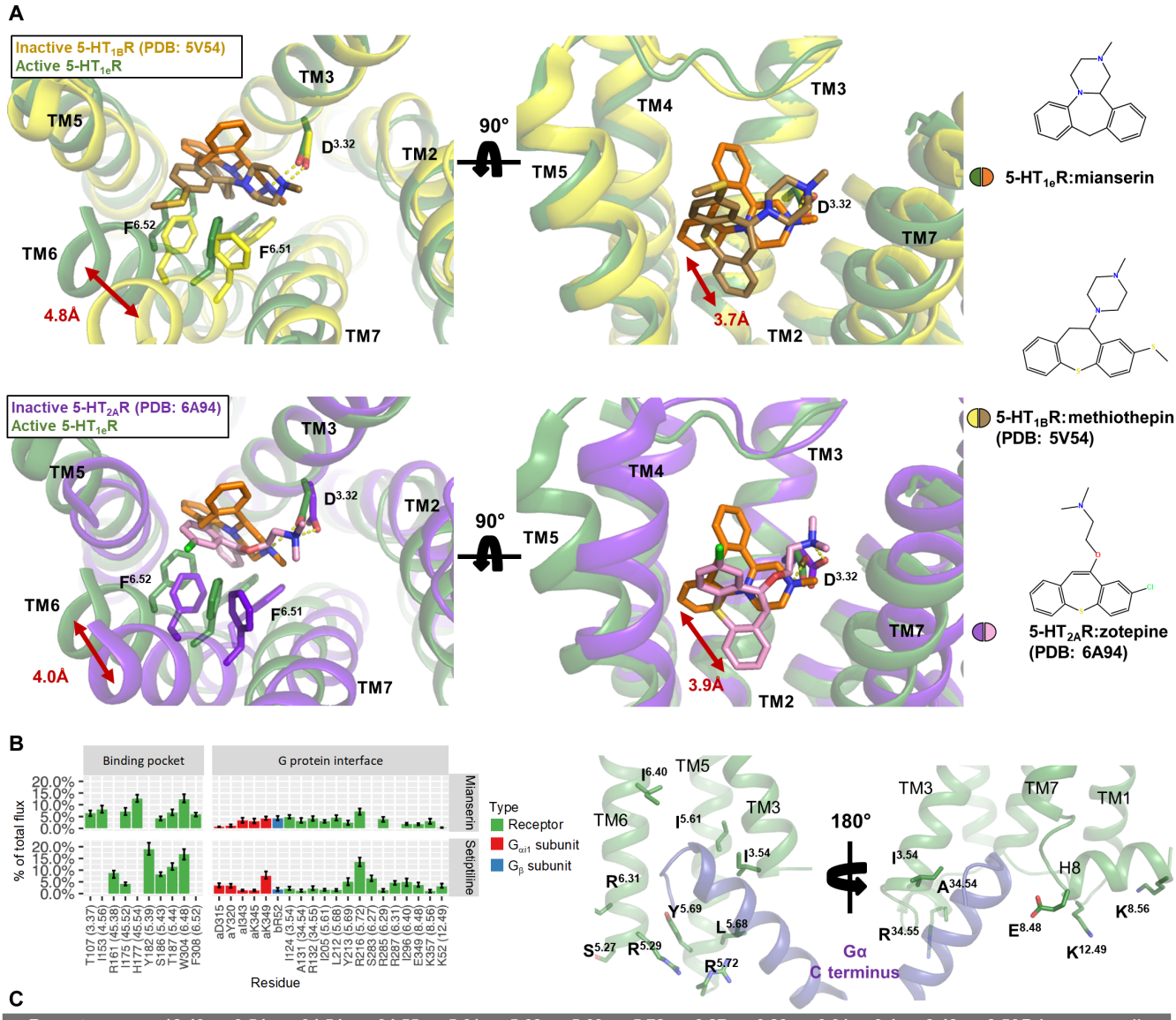

Receptor	12.49	3.54	34.54	34.55	5.61	5.68	5.69	5.72	6.27	6.29	6.31	6.4	8.48	8.56	Primary coupling
5-HT$_{1e}$R	K	I	A	R	I	L	Y	R	S	R	R	I	E	K	$G_{i/o}$
5-HT$_{1F}$R	K	I	A	R	I	L	Y	R	G	R	R	I	E	K	$G_{i/o}$
5-HT$_{1B}$R	K	I	S	A	I	R	I	Q	A	R	R	I	E	K	$G_{i/o}$
5-HT$_{1D}$R	K	I	S	K	I	R	I	P	A	R	R	I	E	K	$G_{i/o}$
5-HT$_{2A}$R	K	I	S	R	T	E	A	C	I	N	Q	V	K	R	$G_{q/11}$
5-HT$_{1A}$R	S	I	V	N	I	R	I	T	L	R	R	I	K	K	$G_{i/o}$
5-HT$_{2C}$R	K	I	S	R	T	Q	A	L	I	N	R	V	K	N	$G_{q/11}$
5-HT$_{5A}$R	T	I	T	-	I	R	V	R	E	K	Q	L	K	N	$G_{i/o}$
5-HT$_{2B}$R	K	I	N	Q	T	K	A	V	I	N	Q	V	K	R	$G_{q/11}$
5-HT$_{7}$R	K	I	P	V	I	S	A	H	F	R	Q	I	R	S	G_{s}
5-HT$_{6}$R	A	I	K	L	I	Q	A	V	S	K	L	L	R	R	G_{s}
5-HT$_{4}$R	Q	I	R	N	I	H	A	I	M	T	T	I	K	I	G_{s}

Fig. 5. Molecular basis of mianserin's and setiptiline's agonism at 5-HT$_{1e}$R. (**A**) Superposition of mianserin-bound 5-HT$_{1e}$R and structures of inactive-state 5-HTRs bound to multicyclic antagonists reveals key differences in drug binding poses. Mianserin–5-HT$_{1e}$R complex is colored in orange and green, methiothepin–5-HT$_{1B}$R complex (PDB: 5V54) is colored in brown and yellow, and zotepine–5-HT$_{2A}$R complex (PDB: 6A94) is colored in pink and purple. Conserved ionic bonds between drugs and D3.32 are indicated as yellow dashed lines. Distances between mianserin and respective antagonists are measured between atoms closest to the 7TM core and shown as red arrows. 2D chemical structures of mianserin, methiothepin, and zotepine are shown on the right. (**B**) Shannon transfer entropy analysis between pairs of ligand-residue or residue-residue contacts within a minimum distance of less than 4.5 Å during MD simulations of mianserin–5-HT$_{1e}$R–G$_{i1}$ and setiptiline–5-HT$_{1e}$R–G$_{i1}$ complexes. Only residues that contribute markedly (>3%) to the transfer entropy between the ligand-binding pocket and the receptor G protein interface in each system are reported. (**C**) Sequence alignment of key residues of 5-HTR family involved in signal transduction.

receptor, suggesting that these interactions contribute to the binding of the ligand but not to the allosterically regulated activation of the receptor. Notably, most of the residues establishing direct interactions with the ligands are conserved within the 5-HT_1R family, except $H177^{ECL2}$ (S190 in 5-HT_{1A} and T203 and T192 in 5-HT_{1B}R and 5-HT_{1D}R, respectively). By contrast, we find that several of the residues contributing to the allosteric communication between the ligand binding pocket and the receptor–G protein interface are different among receptor subtypes (e.g., $R132^{34.55}$ is N146 in 5-HT_{1A}R, A159 in 5-HT_{1B}R, and K148 in 5-HT_{1D}R; $Y213^{5.69}$ is I266, I239, and I228 in 5-HT_{1A}R, 5-HT_{1B}R, and 5-HT_{1D}R, respectively; $R216^{5.72}$ is T229 in 5-HT_{1A}R, E242 in 5-HT_{1B}R, and P231 in 5-HT_{1D}R) (Fig. 5C). This suggests that receptor-specific differences in allosteric communication could further contribute to differences in receptor subtype signaling in the 5-HT_1R family and thus help explain the unexpected agonism of mianserin and setiptiline at 5-HT_{1e}R and 5-HT_{1F}R.

DISCUSSION

Here, we report on the agonistic activity of multiple clinically used drugs, including those of the TeCA class of antidepressants mianserin, setiptiline, and mirtazapine, at the understudied serotonin receptors 5-HT_{1e}R and 5-HT_{1F}R. The finding that similar binding affinities across related cohorts of receptors may not translate to similar pharmacological activities has also previously been noted for other drugs such as D-lysergic acid diethylamide (LSD), which activates most serotonin receptors but is an antagonist at 5-HT_7R (*45*). Our data thus further demonstrate that even within classes of GPCRs tuned to the same endogenous ligand, exogenous drugs have complex pharmacological profiles that cannot be generalized across receptor subtypes without the appropriate testing. Moreover, the polypharmacological profiles of these compounds may result in conflicting or complementary actions within and across circuits or cell types, which warrants further detailed examination.

To investigate the binding modes and activation mechanisms of mianserin and setiptiline, we further determined cryo-EM structures of drug-bound 5-HT_{1e}R signaling complexes and combined our structural analysis with MD simulations and SAR studies. Accordingly, our studies suggest that a distinct binding mode together with receptor-specific allosteric communication between ligand and G protein binding sites are largely responsible for the unexpected agonism of mianserin and setiptiline at 5-HT_{1e}R (and 5-HT_{1F}R). As our tested mutations neither ablate the affinity of mianserin or setiptiline nor convert either of these compounds into 5-HT_{1e}R antagonists, we further posit that the overall ligand-binding pose and downstream allosteric networks, rather than solely specific ligand-receptor interactions, drive drug efficacy, as has been observed for opioid receptors and the β2-adrenergic receptor (*46*, *47*). Notably, the largest impact on efficacy of the TeCA ligands was observed for the mutations $H177^{ECL2}$T and $T330^{7.39}$V, which correspond to the residues at these positions in the 5-HT_2R family. As both mutations in isolation substantially lowered the affinity of 5-HT, it is unlikely that these residues can act alone in determining the efficacy of the TeCA ligands at a given 5-HTR.

The current degree of understanding about what differentiates an antagonist from an agonist at the structural level is relatively underdeveloped. Studies have shown that structural differences in the receptor binding pocket of active- and inactive-state receptors can range from very subtle to markedly different in a highly ligand-specific manner that is difficult to generalize, such as the 5-HT_{2A}R agonists LSD and 25CN-NBOH compared to the antagonist methiothepin (*48*). However, in line with the herein reported findings, we have previously already shown that ergolines that penetrate deeper into the binding pocket of 5-HT_{2B}R confer antagonism relative to chemically similar counterparts that exhibit a shallower binding mode (*49*). Structures of other drug-bound serotonin receptors similarly highlight how deep protrusions into the receptor core and distinct interactions with key activation motifs are key features of antagonists (*40*, *41*, *50*, *51*). In addition, mianserin, setiptiline, and mirtazapine have compact multicyclic scaffolds that span only 2 to 3 atoms between the anchoring amine and the aromatic rings. This likely facilitates contraction of the binding pocket, which is a key feature of GPCR agonism across several receptor classes (*42*, *52*, *53*). However, we also find that even larger multicyclic compounds such as chlorpromazine (Thorazine) can activate 5-HT_{1e}R and 5-HT_{1F}R, albeit with weaker potency compared to mianserin. Together, these findings suggest that the unique topology of the 5-HT_{1e}R and 5-HT_{1F}R ligand-binding pockets allows for distinct positioning of these scaffold classes that facilitate contraction of the pocket and rearrangements in key activation motifs. A conclusive dissection of the mechanisms by which mianserin and setiptiline activate 5-HT_{1e}R and 5-HT_{1F}R, however, will require additional work including the characterization of the receptors' inactive states and/or structural studies of mianserin and setiptiline bound to 5-HTRs they antagonize.

Beyond providing much needed molecular and pharmacological insight into the mechanisms of 5-HT_{1e}R and 5-HT_{1F}R, our studies further have direct clinical implications. For instance, mianserin and mirtazapine have both been observed clinically to relieve migraines, and mirtazapine is now even being used off-label for antimigraine prophylaxis. We thus posit that the drugs' potent agonism of the validated antimigraine target 5-HT_{1F}R contributes to their clinical antimigraine efficacy (*54*, *55*). Similarly, pimethixene showed initial promise as a treatment for migraine, albeit with a poor side effect profile attributed to its high affinity for H_1R histamine receptors and 5-HT_{2C}R serotonin receptors (*23*, *24*). Last, methylergonovine has also shown clinical utility in treating migraine, although its long-term administration is contraindicated due to the potential for fibrotic symptoms as a consequence of 5-HT_{2B}R agonism (*56*).

As for 5-HT_{1e}R, little is known about its (patho)physiological role, outside of recent studies suggesting that the receptor may mediate neuroprotective effects of carboxypeptidase E and that it separately could be a potential drug target for ovarian cancer (*13*, *57*). However, 5-HT_{1e}R is expressed across many brain areas including the basal ganglia, anterior cingulate cortex, and prefrontal cortex. These are key areas for the antidepressant action of increased serotonergic tone, and 5-HT_{1e}R–mediated effects could thus conceivably contribute to the clinical efficacy of the antidepressants mianserin, setiptiline, and mirtazapine. Furthermore, 5-HT_{1e}R's expression in the ovaries and uterus could conceivably play a role in the development of menstruation disorders in response to combining mirtazapine with other selective serotonin reuptake inhibitors (*58*) or contribute to the clinical efficacy of methylergonovine as a uterotonic (*59*). These observations warrant further examination of the role of 5-HT_{1e}R both neurologically and in utero, as well as the clinical effects of the herein described drugs that may, in part, be mediated by 5-HT_{1e}R and/or 5-HT_{1F}R.

Together, our studies not only uncover fundamental details about the unique molecular mechanisms of the enigmatic serotonin receptors 5-HT_{1e}R and 5-HT_{1F}R but also suggest their direct involvement in the physiological effects of various drugs. Given the poorly understood physiological role of 5-HT_{1e}R, we further hope to revitalize medicinal chemistry campaigns oriented around generating selective probes for future in vivo studies.

MATERIALS AND METHODS

Construct design for protein expression

Full-length human 5-HT_{1e}R was cloned into a pFastBac vector similarly to the previously published structure of the receptor, featuring an N-terminal FLAG and 8× His tags followed by a Tobacco Etch Virus (TEV) protease cleavage sequence and an N-terminal b562RIL apocytochrome (BRIL) fusion to improve expression and stability (*33*). In addition, an $L111^{3.41}W$ mutation was added to stabilize 5-HT_{1e}R (*60*). To simplify G protein heterotrimer expression and purification, we used a human $G\gamma_2$-$G\alpha_{i1}$ fusion construct with a GSAGSAGSA sequence linker (gift of T. Che) for formation of heterotrimeric G_{i1}. The setiptiline–5-HT_{1e}R–G_{i1} complex was further stabilized with a separately expressed ScFv16 (*61*). ScFv16 was cloned into a pFastBac vector with an N-terminal gp67 sequence to facilitate its secretion for subsequent purification (*62*). The mianserin–5-HT_{1e}R–G_{i1} complex features a dominant-negative (DNGαi1) construct of Gαi1 containing the mutations S47N, G203A, E245A, and A326S (*63*).

Protein expression

5-HT_{1e}R, $G\gamma_2$-$G\alpha_{i1}$, and $G\beta_1$ were expressed in *Spodoptera frugiperda* (*Sf9*) insect cells (Expression Systems) using the baculovirus method (Expression Systems). For the mianserin–5-HT_{1e}R–G_{i1} complex, receptor and heterotrimeric G protein were expressed and purified separately and assembled subsequently. For the setiptiline–5-HT_{1e}R–G_{i1} complex, receptor and G protein components were coexpressed, and scFv16 was added after complex purification to stabilize the signaling complex. Cell cultures were grown in ESF 921 serum-free medium (Expression Systems) to a density of 2 to 3 million cells/ml and then infected with separate baculoviruses either at a multiplicity of infection of 3 (receptor alone) and 2:2 (Gγ2-Gαi1:Gβ1) in the case of the mianserin complex or at a ratio of 2:1:1 (5-HT_{1e}R:Gγ2-Gαi1:Gβ1) for the setiptiline complex. The culture was collected by centrifugation 48 hours after infection, and cell pellets were stored at −80°C until further use.

Protein purification and complexation

5-HT_{1e}R purification

5-HT_{1e}R–expressing insect cells were disrupted by dounce homogenization in a hypotonic buffer containing 10 mM Hepes (pH 7.5), 10 mM $MgCl_2$, 20 mM KCl, and home-made protease inhibitor cocktail [500 μM "4-(2-aminoethyl)benzenesulfonyl fluoride (AEBSF), 1 μM E-64, 1 μM leupeptin, and 150 nM aprotinin], and membranes were recovered as a pellet following centrifugation at 50,000*g*. Pelleted cellular membranes were homogenized and centrifuged twice in a high osmotic buffer containing 1 M NaCl, 10 mM Hepes (pH 7.4), 10 mM $MgCl_2$, 20 mM KCl, and home-made protease inhibitor cocktail. Purified membranes were subsequently resuspended in a buffer of 150 mM NaCl, 10 mM $MgCl_2$, 20 mM KCl, 20 mM Hepes (pH 7.4), 10 μM mianserin, and home-made protease inhibitor cocktail and agitated at room temperature for 30 min to allow compound binding, before being moved to 4°C. Solubilization was initiated with the addition of solubilization buffer containing 150 mM NaCl, 20 mM Hepes (pH 7.4), 2% *n*-dodecyl-β-D-maltopyranoside (DDM; Anatrace), and 0.4% CHS (cholesteryl hemisuccinate; Anatrace) and allowed to proceed for 2 hours with agitation. Subsequently, insoluble membrane components were removed from solution by centrifugation at 50,000*g*, and the supernatant was supplemented with 20 mM imidazole and incubated overnight with TALON Superflow cobalt affinity resin (Cytiva). TALON resin was washed with buffer 1 [800 mM NaCl, 20 mM Hepes (pH 7.4), 0.1% DDM, 0.02% CHS, 10% glycerol, 20 mM imidazole, and 10 μM mianserin]. The DDM present in the sample was exchanged for lauryl maltose neopentyl glycol (LMNG) by incubating the protein-bound resin with buffer 1 supplemented with 0.1% LMNG for 1 hour at 4°C. The resin was successively washed with the following buffers: wash buffer II [50 mM Hepes (pH 7.5), 800 mM NaCl, 0.05% (w/v) LMNG, and 0.01% (w/v) CHS], wash buffer III [50 mM Hepes (pH 7.5), 800 mM NaCl, 0.01% (w/v) LMNG, and 0.002% (w/v) CHS], and wash buffer IV [25 mM Hepes (pH 7.5), 500 mM NaCl, 0.005% (w/v) LMNG, and 0.001% (w/v) CHS]. Receptor was eluted with 25 mM Hepes (pH 7.5), 500 mM NaCl, 0.005% (w/v) LMNG, 0.001% (w/v) CHS, 10 μM mianserin, and 250 mM imidazole. The eluted proteins were concentrated using Vivaspin 6 Centrifugal Concentrators (Sartorius), and imidazole was removed from the sample using PD Minitrap Sample Preparation Columns (Cytiva). The resulting sample was immediately concentrated and used for complexation.

G_{i1} purification

$G\gamma_2$-$G\alpha_{i1}$/$G\beta_1$–expressing insect cells were dounce-homogenized in a lysis buffer consisting of 20 mM Hepes (pH 7.4), 100 mM NaCl, 1 mM $MgCl_2$, 10 μM guanosine diphosphate (GDP), 10% glycerol, 5 mM β-mercaptoethanol, 30 mM imidazole, 0.2% Triton X-100, and home-made protease inhibitor cocktail. The cytoplasmic and membrane fractions were separated by centrifugation at 50,000*g* for 20 min at 4°C. The resulting supernatant was subjected to an additional centrifugation at 200,000*g* for 45 min at 4°C to further clarify the supernatant. The final supernatant was bound to HisPur Nickel-Nitrilotriacetic Acid (Ni-NTA) resin (Thermo Fisher Scientific) overnight at 4°C.Protein-bound Ni-NTA resin was washed with 20 column volumes (cv) of lysis buffer lacking 0.2% Triton X-100, followed by 20 cv of lysis buffer lacking 0.2% Triton X-100 and 30 mM imidazole. Protein was eluted from the resin with lysis buffer lacking Triton X-100 and supplemented with 300 mM imidazole. The first two elution fractions after the elimination of dead volume were concentrated using Vivaspin 6 Centrifugal Concentrators (Sartorius). Imidazole was removed from the concentrated eluent using PD MiniTrap Sample Preparation Columns (Cytiva) according to the manufacturer's protocol. The N-terminal His tag was removed from the $G\beta_1$ subunit through treatment with PreScission Protease (GenScript). Purified protein and protease were incubated overnight at 4°C to facilitate cleavage. Cleaved proteins were separated from PreScission Protease and uncleaved proteins through a 15-min incubation with TALON resin at 4°C. Cleaved G proteins were concentrated for immediate use or flash frozen and stored at −80°C.

ScFv16 purification

ScFv16-expressing insect cells were pelleted by centrifugation, and the media they were grown in was collected for isolation of protein. Media was treated in sequence with tris (pH 8.0) (to a final concentration of 50 mM), $CaCl_2$ (final concentration of 5 mM), and $CoCl_2$

(final concentration of 1 mM) and stirred at room temperature for 1 hour to precipitate media components. Precipitate was allowed to sediment and further removed by filtration with a 0.22-μm polyethersulfone (PES) Bottle Top Filter (Thermo Fisher Scientific). The final supernatant was supplemented with a final concentration of 10 mM imidazole and stirred with HisPur Ni-NTA resin (Thermo Fisher Scientific) overnight at 4°C. Protein-bound Ni-NTA resin was removed from the supernatant by gradually removing solution from the top after sedimentation and packed into a plastic flow column. Resin was subsequently washed with 10 cv of 20 mM Hepes (pH 7.5), 500 mM NaCl, 10 mM imidazole, and 10% glycerol. Further washing was done with 15 cv of 20 mM Hepes (pH 7.5), 100 mM NaCl, and 10% glycerol. Protein was eluted from the resin with 20 mM Hepes (pH 7.5), 100 mM NaCl, 300 mM imidazole, and 10% glycerol. The eluent was concentrated using Vivaspin 6 Centrifugal Concentrators (Sartorius). Imidazole was removed from the concentrated eluent using PD MiniTrap Sample Preparation Columns (Cytiva) according to the manufacturer's protocol. Desalted protein was concentrated, flash frozen, and stored at −80°C until needed for complexation.

Setiptiline/5-HT$_{1e}$R–G$_{i1}$ complex purification

For the setiptiline-bound 5-HT$_{1e}$R–G$_{i1}$ complex, cell pellets were thawed and resuspended in complex lysis buffer [75 mM NaCl, 10 mM $MgCl_2$, 10 mM $CaCl_2$, 20 mM KCl, 10 mM Hepes (pH 7.4), 10 μM setiptiline, and 10 μM GDP], dounce-homogenized to lyse cells, and subsequently allowed to incubate for 30 min at room temperature with agitation. Apyrase (25 mU/ml; New England Biolabs) was then added, and the mixture was agitated for another 30 min at room temperature, when a twofold molar excess of ScFv16 (estimated from previous purification yields) was added and allowed to mix for another 30 min. The mixture was moved to 4°C, and solubilization was initiated with the addition of solubilization buffer (described above) for 2 hours. Insoluble material was removed by centrifugation at 50,000*g*, and the supernatant containing complex was supplemented with 20 mM imidazole, added to TALON Superflow cobalt affinity resin, and agitated overnight at 4°C. Resin was washed the following day with complex buffer 1 (buffer 1 + 5 mM $MgCl_2$), complex buffer 2 (buffer 2 + 5 mM $MgCl_2$), and eluted with complex buffer 3 (buffer 3 + 5 mM $MgCl_2$). Eluted complex fractions were pooled, concentrated with a Vivaspin 6 Centrifugal Concentrator, supplemented with 1% LMNG, and allowed to sit for an hour at 4°C. Protein was subsequently injected onto a Superdex 200 Increase (Cytiva) size exclusion chromatography column equilibrated in 20 mM Hepes (pH 7.4), 100 mM NaCl, 0.00075% LMNG, 0.00025% glyco-diosgenin (GDN; Anatrace), 0.00015% CHS, and 10 μM setiptiline, and peak fractions containing intact receptor-heterotrimer-ScFv16 complex were collected. Pooled fractions were concentrated and kept on ice until cryo-EM grid preparation.

Mianserin/5-HT$_{1e}$R–G$_{i1}$ complexation and complex purification

To form mianserin-bound 5-HT$_{1e}$R–G$_{i1}$ complexes, purified 5-HT$_{1e}$R and G$_{i1}$ were combined at a molar ratio of 1:1.2 on ice in a buffer with a final composition of 20 mM Hepes (pH 7.4), 120 mM NaCl, 5 mM $CaCl_2$, 2.5 mM $MgCl_2$, 10 μM mianserin, 0.001% (w/v) LMNG, and 0.0002% (w/v) CHS. Complexation was allowed to proceed on ice for an hour and 20 min after which 25 mU per ml apyrase was added, and the complex mixture was incubated overnight at 4°C. The following day, the complex mixture was injected onto a Superdex 200 Increase (Cytiva) size exclusion chromatography column equilibrated in 20 mM Hepes (pH 7.4), 100 mM NaCl, 0.001% LMNG, 0.00025% GDN (Anatrace), 0.0002% CHS, and 10 μM mianserin. Peak fractions containing intact receptor-heterotrimer complex were collected. Pooled fractions were concentrated and kept on ice until cryo-EM grid preparation.

Cryo-EM grids and imaging

Approximately 3 μl of 5-HT$_{1e}$R–G$_{i1}$ complex (at 21 and 9.8 mg/ml for mianserin- and setiptiline-bound complexes, respectively) sample was applied to glow-discharged Quantifoil R 1.2/1.3 300 mesh copper grids, which were subsequently blotted for 3 s and vitrified by plunging into liquid ethane using an EM-GP2 plunge freezer (Leica). Grids were then stored in liquid nitrogen until data collection.

All automatic data collection was performed on a FEI Titan Krios instrument equipped with a Gatan K3 direct electron detector operated by the New York Structural Biology Center (New York, New York). The microscope was operated at 300-kV accelerating voltage, at a nominal magnification of ×64,000 corresponding to a pixel sizes of 1.069 Å (mianserin-bound complex) and 1.076 Å (setiptiline-bound complex). For the mianserin-bound complex, 4141 movies were obtained at a dose rate of 26.27 electrons/Å^2 per second with a defocus ranging from −0.5 to −1.8 μm. The total exposure time was 2 s, and intermediate frames were recorded in 0.05-s intervals, resulting in an accumulated dose of 52.54 electrons/Å^2 and a total of 40 frames per micrograph. For the setiptiline-bound complex, 6935 movies were obtained at a dose rate of 25.77 electrons/Å^2 per second with a defocus ranging from −0.5 to −1.8 μm. The total exposure time was 2 s, and intermediate frames were recorded in 0.05-s intervals, resulting in an accumulated dose of 51.53 electrons/Å^2 and a total of 40 frames per micrograph.

Movies were motion-corrected using MotionCor2 and imported into cryoSPARC (Structura Biotechnology) for further processing. Contrast transfer functions (CTFs) of micrographs were estimated using patchCTF in cryoSPARC. An initial model was produced from a subset of micrographs using blob picking, followed by extraction, two-dimensional (2D) classification, selection of key classes, and generation of a model ab initio. Subsequent models were produced from curated micrograph sets using particles found by template picking using the initial model. Particles were extracted and subjected to 2D classification, and a final particle stack was obtained by iterative rounds of multiclass 3D heterogeneous refinement sorting with several bad densities from rejected particles and the best density from each round of classification. Last, nonuniform refinement was used to further refine the receptor–G protein complexes to their final resolutions—a stack of 1,321,565 particles for the mianserin-bound complex at 3.30 Å and a stack of 221,798 particles for the setiptiline-bound complex at 3.32 Å. In the case of the mianserin-bound complex, we found that further attempts to reduce the particle stack size reduced the global resolution substantially, whereas the setiptiline-bound complex readily split into a small fraction of the particle stack size with a similar resolution.

Model construction and refinement

Model building was conducted in COOT using the published 5-HT$_{1e}$R–G$_{i1}$ complex as a template. Manual adjustments were iteratively performed in alternation with real-space refinement using the real_space_refine PHENIX program to obtain the final refined atomic model, which was validated using MolProbity. The final mianserin- and setiptiline-bound complex models include receptor residues 20 to 160, 170 to 216, and 283 to 358. Poorly resolved residues were modeled as alanines. Ligand models were generated with

the Grade2 webserver (*64*). All structural figures in this text were rendered using PyMOL, except for the overall density map in Fig. 3, and local resolution figures in the supplement, which were made using ChimeraX.

Mammalian cell culture

Human embryonic kidney (HEK) 293T cells and HTLA cells, a modified HEK293T line expressing a modified β-arrestin2 (a gift from B. Roth), were used for assays presented in this work and cultured in Dulbecco's modified Eagle's medium (DMEM; Gibco) supplemented with 10% (v/v) fetal bovine serum (FBS) and 1% (v/v) penicillin-streptomycin (P/S). Intermittently, HTLA cells were cultured with selection media that contained hygromycin (100 μg/ml) and puromycin (2 μg/ml) to maintain the stability of transgenic constructs in the cell line. All cell plates were maintained in a humid 37° incubator with 5% CO_2.

G protein dissociation assays

HEK293T cells were seeded in 10-cm plates or six-well plates, transferred into DMEM containing 1% (v/v) dialyzed FBS (Omega Scientific), and allowed to equilibrate for at least an hour at 37°C. Equilibrated cells were then transfected using DNA/polyethyleneimine (PEI) particles at a 1:2 (w/v) ratio in OptiMEM (Gibco). For cotransfection, we used a ratio of 1:3:3:3 of receptor:Gα:Gβ:Gγ using TRUPATH plasmids (*20*) as well as 5-HT_{1e}R and 5-HT_{1F}R cloned into pcDNA3.1 vectors. On the day following transfection, cells were plated in a white, nontransparent bottom 384-well plate at a density of 10,000 cells per well. The next day, media was exchanged in each well for 30-μl assay buffer [20 mM Hepes (pH 7.4), 0.1% (w/v) bovine serum albumin (BSA), 0.01% (v/v) ascorbic acid, and 1× Hanks' balanced salt solution (Gibco)], and 15 μl of compounds diluted in series in assay buffer was added to the appropriate wells. Cells were incubated for 20 min in a 37°C incubator and then brought to room temperature to incubate for 10 min. Subsequently, 15 μl of 30 μM coelenterazine 400a (GoldBio) in assay buffer was added to all wells, and the plate was immediately read using a multimode fluorescent plate reader (PerkinElmer Victor NIVO). Emission filters were set to 395 nm (RLuc8-coelenterazine 400a) and 510 nm (GFP2) with integration times of 1 s per well. Data were plotted and analyzed using GraphPad Prism 8.0. Functional activity, the G protein dissociation, was determined by calculating the ratio of GFP2 to Rluc8 emission counts. These ratios were then plotted as a function of drug concentration and then analyzed in GraphPad Prism using the nonlinear regression analysis of log(agonist) versus response. Data were then normalized as a percentage of serotonin activation.

cAMP accumulation assays

HEK293T cells were seeded in 10-cm plates, transferred into DMEM containing 1% (v/v) dialyzed FBS, and allowed to equilibrate for at least an hour at 37°C. Equilibrated cells were transfected with a 1:10 ratio of 5-HT_{1e}R or 5-HT_{1F}R to GloSensor plasmid (Promega) using PEI in OptiMEM (Gibco). On the day following transfection, cells were plated in white, transparent bottom 384-well assay plates at a density of 10,000 cells per well. The following day, media was exchanged in each well for assay buffer containing 1.2 mM D-Luciferin (GoldBio). Cells were incubated for at least 1 hour at 37°C before the addition of compounds diluted in series in assay buffer to 3× final concentration. Cells were allowed to incubate in the dark at room temperature for 30 min. Subsequently, 1.6 μM isoproterenol in assay buffer was added to each well to stimulate cAMP production. Cells were incubated in the dark at room temperature for an additional 15 min before being read in a PerkinElmer Trilux Microbeta. Luminescent counts per second (LCPS) were reported and then plotted as a function of drug concentration and analyzed in a nonlinear regression analysis of log(agonist) versus response in GraphPad Prism 8.0.

Arrestin recruitment assays

For β-arrestin2 recruitment, we used the PRESTO-Tango assay, which was performed essentially as described (*17*). The 5-HT_{1e}R and 5-HT_{1F}R PRESTO-Tango constructs were obtained from Addgene. DNA was incubated with PEI in OptiMEM and then added to HEK293T cells in DMEM supplemented with 1% (v/v) dialyzed FBS. After transfection, cells were placed into the 37°C incubator overnight. The following day, cells were plated in DMEM supplemented with 1% (v/v) dialyzed FBS in wells of poly-lysine–coated white, transparent bottom 384-well plates as described above. The cell plates were placed into the 37°C incubator for approximately 4 hours or until cells adhered to the bottom of the plate. Drugs diluted in series to 3× concentration in assay buffer were then added directly to cell media, and the plates were incubated at 37°C overnight for approximately 16 hours. The next day, the drug solution and media were removed and replaced with 20 μl of BrightGlo Reagent (Promega). Cells were incubated in the dark at room temperature for 20 min before being read in a PerkinElmer Trilux Microbeta. LCPS were reported and then plotted as a function of drug concentration and analyzed in a nonlinear regression analysis of log(agonist) versus response in GraphPad Prism 8.0.

Screening analysis

The compound screen tested each indicated compound in quadruplicate at a dose of 10 μM. The quadruplicates were averaged, and the means were normalized against a baseline: Every compound that elicited a response half of a $\log_2$ fold change over baseline was considered active. For the GloSensor Assay, the baseline was set via a control plate, which had cells transfected only with GloSensor, while PRESTO-Tango assays did not use a control plate due to the nature of the assay. For the GloSensor cAMP assay, compounds were considered active that showed a more than $0.5*\log_2$ fold change in signal in receptor-transfected cells compared to cells that were only transfected with the cAMP sensor. For PRESTO-Tango, compounds were considered active that showed a more than $0.5*\log_2$ fold change in signal compared to DMSO. All concentration response experiments reported herein were performed in triplicate and averaged from at least two independent experiments (detailed biological replicate numbers are indicated in figure legends). Data are shown as mean ± SEM. All analyses were done in GraphPad Prism.

Radioligand binding assays

Membrane fractions were prepared from cell lines stably expressing 5-HT_{1e}R and indicated 5-HT_{1e}R mutants. Stable cell lines were generated using the Flp-In 293 T-Rex system (Thermo Fisher Scientific). Cells were grown in 15-cm dishes to 70% confluency in DMEM (Gibco) containing 10% FBS (BioTC), 1% P/S (Gibco), hygromycin B (100 μg/ml; GoldBio), and blasticidin (10 μg/ml; GoldBio). To induce protein expression, the media was changed to DMEM containing 1% dialyzed FBS, 1% P/S, and tetracycline (2 μg/ml; Sigma-Aldrich). The cells were allowed to grow for an additional 24 hours. The media was

replaced with fresh DMEM containing 1% dialyzed FBS, 1% P/S, and tetracycline (2 μg/ml), and the cells were incubated for an additional 24 hours. Following induction, cells were harvested by washing twice with phosphate-buffered saline (Gibco) and lysed in a hypotonic buffer [10 mM Hepes (pH 7.5), 2 mM EDTA, and homemade protease inhibitor cocktail] on ice. Membrane fractions were isolated from the cell lysate by centrifugation at 4°C for 20 min at 20,000*g*. Each 15-cm plate yielded 10 membrane fraction pellets. Membranes were frozen with liquid nitrogen and stored at −80°C until use.

Saturation binding was performed on membrane pellets in standard binding buffer [50 mM tris (pH 7.5), 10 mM $MgCl_2$, 0.1 mM EDTA with 0.1% BSA, and 0.01% ascorbic acid] using varying concentrations of [^{3}H]5-HT (American Radiolabeled Chemicals, ART 1551-250 μCi). Binding assays were performed in 96-well plates incubated at room temperature for 80 min. Nonspecific binding was determined by the addition of a final concentration of 10 μM methiothepin (Sigma-Aldrich). The experiment was terminated by filtration with a Microbeta Filtermate 96-well Harvester (PerkinElmer) onto glass fiber filters (PerkinElmer, 1450-421) soaked in 0.3% (w/v) polyethyleneimine (Sigma-Aldrich). Filters were washed three times with cold wash buffer [50 mM tris (pH 7.5)] and allowed to dry under vacuum. MeltiLex-A scintillant (PerkinElmer, 1450-441) was melted onto the filters. Counts were determined in a Wallac Trilux Microbeta 1450 (PerkinElmer). K_D values were determined in GraphPad Prism (one site—total and nonspecific binding).

For competition binding, membrane fractions were resuspended in standard binding buffer and incubated in 96-well plates with a single concentration of [^{3}H]5-HT between 3.6 and 8.6 nM and varying concentrations of cold ligand. The plates were incubated at room temperature for 80 min using the same termination and counting procedure described for the saturation binding. K_i values were determined in GraphPad Prism (one site—fit K_i) using the K_D values from corresponding saturation binding experiments. Experiments were normalized by total protein amounts per well as determined by the BCA assay (Thermo Fisher Scientific) according to the manufacturer's protocol.

System setup for MD simulations

The cryo-EM structures of human 5-HT_{1e}R in complex with $G\alpha_{i1}\beta_1\gamma_2$ and bound to mianserin or setiptiline were used as starting points for MD simulations after adding atomic coordinates of the missing ECL2, which was built ab initio with RoseTTAFold (*65*). The N-terminal, C-terminal, and intracellular loop 3 regions of 5-HT_{1e}R, which were missing from the two cryo-EM structures, were not included in the modeling and the simulations. Instead, the truncated receptors were capped with acetyl- and *N*-methyl groups at the N and C terminus, respectively. While the missing short Leu234-Met240 loop of $G\alpha_{i1}$ was built ab initio with RoseTTAFold, the missing N-terminal and Ile55-Thr181 regions of $G\alpha_{i1}$, as well as N- and C-terminal regions of the β and γ subunits of G_i, were not included and their ends capped with acetyl- and *N*-methyl groups, respectively. The Protein Preparation Wizard tool (*66*) of Maestro v. 12.6 (Schrödinger) was used to assign bond orders and add cap terminal groups and missing hydrogens to both the receptor and G protein, as well as most probable protonation states according to a pH of 7.4. Following the PROtein pKa (PROPKA) (*67*) hydrogen bond network optimization protocol at pH 7.4, the protein systems underwent restrained energy minimization using the OPLS3e force field (*68*) and default parameters until the RMSD of the protein heavy atoms reached a value of 0.3 Å.

The 3D structure of S(+)-mianserin was obtained from the Cambridge Crystallographic Data Centre website. S(+)-mianserin and setiptiline ligands with the most probable protonation states at pH of 7.4 were prepared using the default LigPrep protocol in the Schrödinger software release 2020-4 using OPLS3e partial charges (*68*). The dihedral parameters of S(+)-mianserin and setiptiline that were not included in the standard OPLS3e force field were generated using the Force Field Builder (FFBuilder) tool of the Schrödinger suite.

MD simulations

Each ligand-bound receptor system was embedded in a 1-palmitoyl -2-oleoylphosphatidylcholine bilayer, solvated in an orthorhombic box using the Simple Point-Charge (SPC) water model (*69*–*71*) with a 10-Å distance in each cartesian direction between the protein and box boundaries, and neutralized with Na^+ and Cl^- ions. A concentration of 0.15 M NaCl was added to mimic physiological conditions. The OPLS3e force field was used for system preparation using the Desmond System Builder tool of Maestro (*72*).

MD simulations were run using Desmond's default simulation parameters, including a 2-fs time step for bonded forces and short-range nonbonded forces and a 6-fs time step for long-range nonbonded forces using the reversible reference system propagation algorithm integrator. Following the standard membrane relaxation protocol in Desmond, constant-pressure and constant-temperature (NPC; Number of particles, Pressure, and Temperature) equilibration runs were carried out in nine steps, the first eight of which using gradually relaxing positional restraints on the heavy atoms of lipids, protein side chains, protein backbone, ligand ring atoms, and, lastly, the remaining ligand atoms. The last equilibration step consisted of a 1-ns unrestrained NPT run. During equilibration, the system temperature and pressure were maintained at 300 K and 1 bar, respectively, using the Nose-Hoover thermostat (*73*) and a semi-isotropic Martyna, Tobias, and Klein barostat. Short-range coulomb interactions were cut at 9 Å.

Four independent 250-ns MD production runs were carried out for each ligand-receptor complex, and structural data were collected every 0.5 ns. The resulting 2000 frames for each system were stripped of the ions and lipids before aligning the heavy atoms of their respective energy-minimized five HT_{1e}R cryo-EM structures and calculating their RMSD for both the receptor and the ligand's heavy atoms, using an in-house Python script.

SIFt analyses

SIFt analyses (*74*) were performed on the merged MD simulation trajectories using an in-house Python script. The interactions between ligands and receptor residues—both backbone and side chains—were calculated as a 9-bit representation based on (i) hydrogen bond interactions with the protein as the hydrogen bond donor (Hbond_proD) or hydrogen bond acceptor (Hbond_proA), (ii) apolar interactions (carbon-carbon atoms in contact), (iii) face-to-face (Aro_F2F) and edge-to-face (Aro_E2F) aromatic interactions, (iv) electrostatic interactions with positively (Elec_ProP) or negatively charged (Elec_ProN) residues, and (v) one-water–mediated hydrogen bond (Hbond_1wat) or two-water–mediated hydrogen bonds (Hbond_2wat). A distance cutoff of 4.5 Å was used to define apolar interactions, a cutoff of 4 Å was used to describe aromatic and electrostatic interactions, and a cutoff of 3.5 Å was used to describe H-bond interactions. The

probability of each interaction was estimated using a two-state Markov model and sampling the transition matrix posterior distribution using standard Dirichlet priors for the transition probabilities as described (*75*).

Transfer entropy analyses

To elucidate the information flow across each simulated ligand-bound 5-HT_{1e}R–$G\alpha_{i1}\beta_1\gamma_2$ system, we calculated the Shannon transfer entropy (*76*) between pairs of ligand-residue or residue-residue contacts within a minimum distance of less than 4.5 Å during MD simulations. Specifically, transfer entropy values were obtained with the MDEntropy package (*77*) between 14 ligand-residue and 696 residue-residue contacts in the case of the mianserin-bound system and 12 ligand-residue and 643 residue-residue contacts in the case of the setiptiline-bound system, yielding transfer entropy matrices of 710 and 655 structural descriptors, respectively. The NetworkX Python library (*78*) was used to build a directed graph in which each node represented a direct ligand-residue or residue-residue contact and the "length" of the edge between two nodes corresponded to the negative logarithm of the transfer entropy between them. The information flow from the ligand orthosteric binding site to the receptor–G protein interface was described by the set of paths Γ connecting the set of ligand-residue contacts (source set) to the set of contacts between receptor and G protein residues (target set). The flux F_γ through each path was calculated as the total length of the path, and the contribution C_k of each node k to the allosteric communication between the ligand binding pocket and the receptor–G protein interface was measured by normalizing the flux and summing over all paths going through that node as

$$C_k = \frac{\sum_{\{\gamma:k\in\gamma\}} F_\gamma}{\sum_{\gamma\in\Gamma} F_\gamma}$$

To assess the contribution of each residue to the allosteric mechanism, we calculated the sum of the contributions of all the nodes that contained that residue. Only residues that contributed the most to allosteric communication (>3% flux) were considered.

Supplementary Materials

This PDF file includes:

Figs. S1 to S13
Tables S1 to S6

REFERENCES AND NOTES

1. N. M. Barnes, G. P. Ahern, C. Becamel, J. Bockaert, M. Camilleri, S. Chaumont-Dubel, S. Claeysen, K. A. Cunningham, K. C. Fone, M. Gershon, G. D. Giovanni, N. M. Goodfellow, A. L. Halberstadt, R. M. Hartley, G. Hassaine, K. Herrick-Davis, R. Hovius, E. Lacivita, E. K. Lambe, M. Leopoldo, F. O. Levy, S. C. R. Lummis, P. Marin, L. Maroteaux, A. C. McCreary, D. L. Nelson, J. F. Neumaier, A. Newman-Tancredi, H. Nury, A. Roberts, B. L. Roth, A. Roumier, G. J. Sanger, M. Teitler, T. Sharp, C. M. Villalón, H. Vogel, S. W. Watts, D. Hoyer, International Union of Basic and Clinical Pharmacology. CX. Classification of receptors for 5-hydroxytryptamine; pharmacology and function. *Pharmacol. Rev.* **73**, 310–520 (2021).
2. M. Berger, J. A. Gray, B. L. Roth, The expanded biology of serotonin. *Annu. Rev. Med.* **60**, 355–366 (2009).
3. K. Sriram, P. A. Insel, G protein-coupled receptors as targets for approved drugs: How many targets and how many drugs? *Mol. Pharmacol.* **93**, 251–258 (2018).
4. A. L. Garcia-Garcia, A. Newman-Tancredi, E. D. Leonardo, 5-HT_{1A} receptors in mood and anxiety: Recent insights into autoreceptor versus heteroreceptor function. *Psychopharmacology* **231**, 623–636 (2014).
5. S. J. Tepper, A. M. Rapoport, F. D. Sheftell, Mechanisms of action of the 5-HT1B/1D receptor agonists. *Arch. Neurol.* **59**, 1084–1088 (2002).
6. X. Qin, J. Li, S. Wang, J. Lv, F. Luan, Y. Liu, Y. Chen, X. Chen, Y. Zhao, J. Zhu, Y. Piao, W. Zhang, Y. Shi, R. Xiang, P. Qu, L. Wang, Serotonin/HTR1E signaling blocks chronic stress-promoted progression of ovarian cancer. *Theranostics* **11**, 6950–6965 (2021).
7. V. K. Sharma, X. Yang, S.-K. Kim, A. Mafi, D. Saiz-Sanchez, P. Villanueva-Anguita, L. Xiao, A. Inoue, W. A. Goddard III, Y. P. Loh, Novel interaction between neurotrophic factor-α1/carboxypeptidase E and serotonin receptor, 5-HTR1E, protects human neurons against oxidative/neuroexcitotoxic stress via β-arrestin/ERK signaling. *Cell. Mol. Life Sci.* **79**, 24 (2021).
8. M. Dukat, C. Smith, K. Herrick-Davis, M. Teitler, R. A. Glennon, Binding of tryptamine analogs at h5-HT1E receptors: A structure-affinity investigation. *Bioorg. Med. Chem.* **12**, 2545–2552 (2004).
9. M. T. Klein, M. Dukat, R. A. Glennon, M. Teitler, Toward selective drug development for the human 5-hydroxytryptamine 1E receptor: A comparison of 5-hydroxytryptamine 1E and 1F receptor structure-affinity relationships. *J. Pharmacol. Exp. Ther.* **337**, 860–867 (2011).
10. V. K. Sharma, Y. P. Loh, The discovery, structure, and function of 5-HTR1E serotonin receptor. *Cell Commun. Signal.* **21**, 235 (2023).
11. S. Huang, P. Xu, Y. Tan, C. You, Y. Zhang, Y. Jiang, H. E. Xu, Structural basis for recognition of anti-migraine drug lasmiditan by the serotonin receptor 5-HT1F-G protein complex. *Cell Res.* **31**, 1036–1038 (2021).
12. B. L. Roth, E. Lopez, S. Patel, W. K. Kroeze, The multiplicity of serotonin receptors: Uselessly diverse molecules or an embarrassment of riches? *Neuroscientist* **6**, 252–262 (2000).
13. Y. Belotti, S. Tolomeo, R. Yu, W.-T. Lim, C. T. Lim, Prognostic neurotransmitter receptors genes are associated with immune response, inflammation and cancer hallmarks in brain tumors. *Cancer* **14**, 2544 (2022).
14. V. K. Sharma, K. Campbell, X. Yang, R. Dale, Y. P. Loh, Characterization of serotonin-5-HTR1E signaling pathways and its role in cell survival. *FASEB J.* **37**, e22925 (2023).
15. B. A. Kumar, P. Kumari, C. Sona, P. N. Yadav, GloSensor assay for discovery of GPCR-selective ligands. *Methods Cell Biol.* **142**, 27–50 (2017).
16. D. Wacker, R. C. Stevens, B. L. Roth, How ligands illuminate GPCR molecular pharmacology. *Cell* **170**, 414–427 (2017).
17. W. K. Kroeze, M. F. Sassano, X.-P. Huang, K. Lansu, J. D. McCorvy, P. M. Giguère, N. Sciaky, B. L. Roth, PRESTO-Tango as an open-source resource for interrogation of the druggable human GPCRome. *Nat. Struct. Mol. Biol.* **22**, 362–369 (2015).
18. G. Barnea, W. Strapps, G. Herrada, Y. Berman, J. Ong, B. Kloss, R. Axel, K. J. Lee, The genetic design of signaling cascades to record receptor activation. *Proc. Natl. Acad. Sci. U.S.A.* **105**, 64–69 (2008).
19. V. Lewis, E. M. Bonniwell, J. K. Lanham, A. Ghaffari, H. Sheshbaradaran, A. B. Cao, M. M. Calkins, M. A. Bautista-Carro, E. Arsenault, A. Telfer, F.-F. Taghavi-Abkuh, N. J. Malcolm, F. El Sayegh, A. Abizaid, Y. Schmid, K. Morton, A. L. Halberstadt, A. Aguilar-Valles, J. D. McCorvy, A non-hallucinogenic LSD analog with therapeutic potential for mood disorders. *Cell Rep.* **42**, 112203 (2023).
20. R. H. J. Olsen, J. F. DiBerto, J. G. English, A. M. Glaudin, B. E. Krumm, S. T. Slocum, T. Che, A. C. Gavin, J. D. McCorvy, B. L. Roth, R. T. Strachan, TRUPATH, an open-source biosensor platform for interrogating the GPCR transducerome. *Nat. Chem. Biol.* **16**, 841–849 (2020).
21. S. Borland, M. Guzman, R. Fishman, T. Armer, Novel receptor activity mapping of methysergide and its metabolite, methylergometrine, provides a mechanistic rationale for both the clinically observed efficacy and risk of fibrosis in patients with migraine (4350). *Neurology* **96**, 10.1212/WNL.96.15_supplement.4350 (2021).
22. P. Schoeffter, D. Hoyer, Interaction of the α-adrenoceptor agonist oxymetazoline with serotonin 5-HT1A, 5-HT1B, 5-HT1C and 5-HT1D receptors. *Eur. J. Pharmacol.* **196**, 213–216 (1991).
23. B. Schmitz, C. Ullmer, D. Segelcke, M. Gwarek, X.-R. Zhu, H. Lübbert, BF-1 – A novel selective 5-HT2B receptor antagonist blocking neurogenic dural plasma protein extravasation in guinea pigs. *Eur. J. Pharmacol.* **751**, 73–80 (2015).
24. T. Dalsgaard-Nielsen, Therapeutic results of prophylactic treatment for "classic" migraine with antaminic substance (B P 400 Sandoz). *Headache* **8**, 6–15 (1968).
25. R. M. Pinder, Mianserin: Pharmacological and clinical correlates. *Nord. Psykiatr. Tidsskr.* **45**, 13–26 (1991).
26. T. Duka, "Mianserin" in *Encyclopedia of Psychopharmacology*, I. P. Stolerman, Ed. (Springer, Berlin, Heidelberg, 2010; https://doi.org/10.1007/978-3-540-68706-1_1845), pp. 769–769.
27. M. C. Olianas, S. Dedoni, P. Onali, The atypical antidepressant mianserin exhibits agonist activity at κ-opioid receptors. *Br. J. Pharmacol.* **167**, 1329–1341 (2012).
28. M. Teitler, N. Toohey, J. A. Knight, M. T. Klein, C. Smith, Clozapine and other competitive antagonists reactivate risperidone-inactivated h5-HT7 receptors: Radioligand binding

and functional evidence for GPCR homodimer protomer interactions. *Psychopharmacology* **212**, 687–697 (2010).
29. E. B. Nascimento Jr., J. G. T. Seniuk, A. M. Godin, W. C. Ferreira, M. B. Dutra, A. C. P. Oliveira, L. F. S. Bastos, B. L. Fiebich, M. M. Coelho, Peripheral 5-HT1B and 5-HT2A receptors mediate the nociceptive response induced by 5-hydroxytryptamine in mice. *Pharmacol. Biochem. Behav.* **99**, 598–603 (2011).
30. M. Protti, R. Mandrioli, C. Marasca, A. Cavalli, A. Serretti, L. Mercolini, New-generation, non-SSRI antidepressants: Drug-drug interactions and therapeutic drug monitoring. Part 2: NaSSAs, NRIs, SNDRIs, MASSAs, NDRIs, and others. *Med. Res. Rev.* **40**, 1794–1832 (2020).
31. P. K. Gillman, Tricyclic antidepressant pharmacology and therapeutic drug interactions updated. *Br. J. Pharmacol.* **151**, 737–748 (2007).
32. A. Schotte, P. F. Janssen, W. Gommeren, W. H. Luyten, P. Van Gompel, A. S. Lesage, K. De Loore, J. E. Leysen, Risperidone compared with new and reference antipsychotic drugs: In vitro and in vivo receptor binding. *Psychopharmacology* **124**, 57–73 (1996).
33. P. Xu, S. Huang, H. Zhang, C. Mao, X. E. Zhou, X. Cheng, I. A. Simon, D.-D. Shen, H.-Y. Yen, C. V. Robinson, K. Harpsøe, B. Svensson, J. Guo, H. Jiang, D. E. Gloriam, K. Melcher, Y. Jiang, Y. Zhang, H. E. Xu, Structural insights into the lipid and ligand regulation of serotonin receptors. *Nature* **592**, 469–473 (2021).
34. V. Isberg, C. de Graaf, A. Bortolato, V. Cherezov, V. Katritch, F. H. Marshall, S. Mordalski, J.-P. Pin, R. C. Stevens, G. Vriend, D. E. Gloriam, Generic GPCR residue numbers - Aligning topology maps while minding the gaps. *Trends Pharmacol. Sci.* **36**, 22–31 (2015).
35. T. Saarenpää, V.-P. Jaakola, A. Goldman, Baculovirus-mediated expression of GPCRs in insect cells. *Methods Enzymol.* **556**, 185–218 (2015).
36. J. D. McCorvy, B. L. Roth, Structure and function of serotonin G protein-coupled receptors. *Pharmacol. Ther.* **150**, 129–142 (2015).
37. O. B. Sanchez-Reyes, G. Zilberg, J. D. McCorvy, D. Wacker, Molecular insights into GPCR mechanisms for drugs of abuse. *J. Biol. Chem.* **299**, 105176 (2023).
38. A. Egyed, D. J. Kiss, G. M. Keserű, The impact of the secondary binding pocket on the pharmacology of class A GPCRs. *Front. Pharmacol.* **13**, (2022).
39. Y. Tan, P. Xu, S. Huang, G. Yang, F. Zhou, X. He, H. Ma, H. E. Xu, Y. Jiang, Structural insights into the ligand binding and Gi coupling of serotonin receptor 5-HT5A. *Cell Discov.* **8**, 50 (2022).
40. K. T. Kimura, H. Asada, A. Inoue, F. M. N. Kadji, D. Im, C. Mori, T. Arakawa, K. Hirata, Y. Nomura, N. Nomura, J. Aoki, S. Iwata, T. Shimamura, Structures of the 5-HT2A receptor in complex with the antipsychotics risperidone and zotepine. *Nat. Struct. Mol. Biol.* **26**, 121–128 (2019).
41. W. Yin, X. E. Zhou, D. Yang, P. W. de Waal, M. Wang, A. Dai, X. Cai, C.-Y. Huang, P. Liu, X. Wang, Y. Yin, B. Liu, Y. Zhou, J. Wang, H. Liu, M. Caffrey, K. Melcher, Y. Xu, M.-W. Wang, H. E. Xu, Y. Jiang, Crystal structure of the human 5-HT1B serotonin receptor bound to an inverse agonist. *Cell Discov.* **4**, 12 (2018).
42. S. G. F. Rasmussen, B. T. DeVree, Y. Zou, A. C. Kruse, K. Y. Chung, T. S. Kobilka, F. S. Thian, P. S. Chae, E. Pardon, D. Calinski, J. M. Mathiesen, S. T. A. Shah, J. A. Lyons, M. Caffrey, S. H. Gellman, J. Steyaert, G. Skiniotis, W. I. Weis, R. K. Sunahara, B. K. Kobilka, Crystal structure of the β2 adrenergic receptor-Gs protein complex. *Nature* **477**, 549–555 (2011).
43. Y. Zhuang, P. Xu, C. Mao, L. Wang, B. Krumm, X. E. Zhou, S. Huang, H. Liu, X. Cheng, X.-P. Huang, D.-D. Shen, T. Xu, Y.-F. Liu, Y. Wang, J. Guo, Y. Jiang, H. Jiang, K. Melcher, B. L. Roth, Y. Zhang, C. Zhang, H. E. Xu, Structural insights into the human D1 and D2 dopamine receptor signaling complexes. *Cell* **184**, 931–942.e18 (2021).
44. J. Holze, M. Bermudez, E. M. Pfeil, M. Kauk, T. Bödefeld, M. Irmen, C. Matera, C. Dallanoce, M. De Amici, U. Holzgrabe, G. M. König, C. Tränkle, G. Wolber, R. Schrage, K. Mohr, C. Hoffmann, E. Kostenis, A. Bock, Ligand-specific allosteric coupling controls G-protein-coupled receptor signaling. *ACS Pharmacol. Transl. Sci.* **3**, 859–867 (2020).
45. D. Wacker, C. Wang, V. Katritch, G. W. Han, X.-P. Huang, E. Vardy, J. D. McCorvy, Y. Jiang, M. Chu, F. Y. Siu, W. Liu, H. E. Xu, V. Cherezov, B. L. Roth, R. C. Stevens, Structural features for functional selectivity at serotonin receptors. *Science* **340**, 615–619 (2013).
46. A. K. Shukla, Structural basis of partial agonism at the β2-adrenergic receptor. *Biochemistry* **58**, 137–139 (2019).
47. R. Uprety, T. Che, S. A. Zaidi, S. G. Grinnell, B. R. Varga, A. Faouzi, S. T. Slocum, A. Allaoa, A. Varadi, M. Nelson, S. M. Bernhard, E. Kulko, V. Le Rouzic, S. O. Eans, C. A. Simons, A. Hunkele, J. Subrath, Y. X. Pan, J. A. Javitch, J. P. McLaughlin, B. L. Roth, G. W. Pasternak, V. Katritch, S. Majumdar, Controlling opioid receptor functional selectivity by targeting distinct subpockets of the orthosteric site. *eLife* **10**, e56519 (2021).
48. K. Kim, T. Che, O. Panova, J. F. DiBerto, J. Lyu, B. E. Krumm, D. Wacker, M. J. Robertson, A. B. Seven, D. E. Nichols, B. K. Shoichet, G. Skiniotis, B. L. Roth, Structure of a hallucinogen-activated Gq-coupled 5-HT2A serotonin receptor. *Cell* **182**, 1574–1588.e19 (2020).
49. J. D. McCorvy, D. Wacker, S. Wang, B. Agegnehu, J. Liu, K. Lansu, A. R. Tribo, R. H. J. Olsen, T. Che, J. Jin, B. L. Roth, Structural determinants of 5-HT2B receptor activation and biased agonism. *Nat. Struct. Mol. Biol.* **25**, 787–796 (2018).
50. Z. Chen, L. Fan, H. Wang, J. Yu, D. Lu, J. Qi, F. Nie, Z. Luo, Z. Liu, J. Cheng, S. Wang, Structure-based design of a novel third-generation antipsychotic drug lead with potential antidepressant properties. *Nat. Neurosci.* **25**, 39–49 (2022).
51. Y. Peng, J. D. McCorvy, K. Harpsøe, K. Lansu, S. Yuan, P. Popov, L. Qu, M. Pu, T. Che, L. F. Nikolajsen, X.-P. Huang, Y. Wu, L. Shen, W. E. Bjørn-Yoshimoto, K. Ding, D. Wacker, G. W. Han, J. Cheng, V. Katritch, A. A. Jensen, M. A. Hanson, S. Zhao, D. E. Gloriam, B. L. Roth, R. C. Stevens, Z.-J. Liu, 5-HT2C receptor structures reveal the structural basis of GPCR polypharmacology. *Cell* **172**, 719–730.e14 (2018).
52. A. C. Kruse, A. M. Ring, A. Manglik, J. Hu, K. Hu, K. Eitel, H. Hübner, E. Pardon, C. Valant, P. M. Sexton, A. Christopoulos, C. C. Felder, P. Gmeiner, J. Steyaert, W. I. Weis, K. C. Garcia, J. Wess, B. K. Kobilka, Activation and allosteric modulation of a muscarinic acetylcholine receptor. *Nature* **504**, 101–106 (2013).
53. T. Che, S. Majumdar, S. A. Zaidi, P. Ondachi, J. D. McCorvy, S. Wang, P. D. Mosier, R. Uprety, E. Vardy, B. E. Krumm, G. W. Han, M.-Y. Lee, E. Pardon, J. Steyaert, X.-P. Huang, R. T. Strachan, A. R. Tribo, G. W. Pasternak, F. I. Carroll, R. C. Stevens, V. Cherezov, V. Katritch, D. Wacker, B. L. Roth, Structure of the nanobody-stabilized active state of the kappa opioid receptor. *Cell* **172**, 55–67.e15 (2018).
54. P. Monro, C. Swade, A. Coppen, Mianserin in the prophylaxis of migraine: A double-blind study. *Acta Psychiatr. Scand. Suppl.* **320**, 98–103 (1985).
55. E. Lévy, H. C. Margolese, Migraine headache prophylaxis and treatment with low-dose mirtazapine. *Int. Clin. Psychopharmacol.* **18**, 301–303 (2003).
56. N. Haque, N. Tariq, Short term oral methylergonovine maleate prophylaxis for status migrainosus. Case series and review of literature. *Front. Neurol.* **10**, 201 (2019).
57. L. Xiao, Y. P. Loh, Neurotrophic factor-α1/carboxypeptidase E functions in neuroprotection and alleviates depression. *Front. Mol. Neurosci.* **15**, 918852 (2022).
58. F. Uguz, M. Sahingoz, S. A. Kose, O. Ozbebit, C. Sengul, Y. Selvi, C. B. Sengul, M. G. Ayhan, A. Dagistanli, R. Askin, Antidepressants and menstruation disorders in women: A cross-sectional study in three centers. *Gen. Hosp. Psychiatry* **34**, 529–533 (2012).
59. C. Vallera, L. O. Choi, C. M. Cha, R. W. Hong, Uterotonic Medications: Oxytocin, Methylergonovine, Carboprost, Misoprostol. *Anesthesiol. Clin.* **35**, 207–219 (2017).
60. C. B. Roth, M. A. Hanson, R. C. Stevens, Stabilization of the human beta2-adrenergic receptor TM4-TM3-TM5 helix interface by mutagenesis of Glu122(3.41), a critical residue in GPCR structure. *J. Mol. Biol.* **376**, 1305–1319 (2008).
61. S. Maeda, A. Koehl, H. Matile, H. Hu, D. Hilger, G. F. X. Schertler, A. Manglik, G. Skiniotis, R. J. P. Dawson, B. K. Kobilka, Development of an antibody fragment that stabilizes GPCR/G-protein complexes. *Nat. Commun.* **9**, 3712 (2018).
62. C. N. Deshpande, V. Xin, Y. Lu, T. Savage, G. J. Anderson, M. Jormakka, Large scale expression and purification of secreted mouse hephaestin. *PLOS ONE* **12**, e0184366 (2017).
63. Y.-L. Liang, P. Zhao, C. Draper-Joyce, J.-A. Baltos, A. Glukhova, T. T. Truong, L. T. May, A. Christopoulos, D. Wootten, P. M. Sexton, S. G. B. Furness, Dominant negative G proteins enhance formation and purification of agonist-GPCR-G protein complexes for structure determination. *ACS Pharmacol. Transl. Sci.* **1**, 12–20 (2018).
64. O. S. Smart, A. Sharff, J. Holstein, T. O. Womack, C. Flensburg, P. Keller, W. Paciorek, C. Vonrhein, G. Bricogne, Grade2 version 1.4.1, Global Phasing Ltd. (2021).
65. M. Baek, F. DiMaio, I. Anishchenko, J. Dauparas, S. Ovchinnikov, G. R. Lee, J. Wang, Q. Cong, L. N. Kinch, R. D. Schaeffer, C. Millán, H. Park, C. Adams, C. R. Glassman, A. DeGiovanni, J. H. Pereira, A. V. Rodrigues, A. A. van Dijk, A. C. Ebrecht, D. J. Opperman, T. Sagmeister, C. Buhlheller, T. Pavkov-Keller, M. K. Rathinaswamy, U. Dalwadi, C. K. Yip, J. E. Burke, K. C. Garcia, N. V. Grishin, P. D. Adams, R. J. Read, D. Baker, Accurate prediction of protein structures and interactions using a three-track neural network. *Science* **373**, 871–876 (2021).
66. G. M. Sastry, M. Adzhigirey, T. Day, R. Annabhimoju, W. Sherman, Protein and ligand preparation: Parameters, protocols, and influence on virtual screening enrichments. *J. Comput. Aided Mol. Des.* **27**, 221–234 (2013).
67. M. H. M. Olsson, C. R. Søndergaard, M. Rostkowski, J. H. Jensen, PROPKA3: Consistent treatment of internal and surface residues in empirical pKa predictions. *J. Chem. Theory Comput.* **7**, 525–537 (2011).
68. K. Roos, C. Wu, W. Damm, M. Reboul, J. M. Stevenson, C. Lu, M. K. Dahlgren, S. Mondal, W. Chen, L. Wang, R. Abel, R. A. Friesner, E. D. Harder, OPLS3e: Extending force field coverage for drug-like small molecules. *J. Chem. Theory Comput.* **15**, 1863–1874 (2019).
69. H. J. C. Berendsen, J. R. Grigera, T. P. Straatsma, The missing term in effective pair potentials. *J. Phys. Chem.* **91**, 6269–6271 (1987).
70. K. Takemura, A. Kitao, Water model tuning for improved reproduction of rotational diffusion and NMR spectral density. *J. Phys. Chem. B* **116**, 6279–6287 (2012).
71. H. J. C. Berendsen, J. P. M. Postma, W. F. van Gunsteren, J. Hermans, "Interaction Models for Water in Relation to Protein Hydration" in *Intermolecular Forces: Proceedings of the Fourteenth Jerusalem Symposium on Quantum Chemistry and Biochemistry Held in Jerusalem, Israel, April 13–16, 1981*, B. Pullman, Ed. (Springer Netherlands, Dordrecht, 1981; https://doi.org/10.1007/978-94-015-7658-1_21) *The Jerusalem Symposia on Quantum Chemistry and Biochemistry*, pp. 331–342.
72. K. J. Bowers, D. E. Chow, H. Xu, R. O. Dror, M. P. Eastwood, B. A. Gregersen, J. L. Klepeis, I. Kolossvary, M. A. Moraes, F. D. Sacerdoti, J. K. Salmon, Y. Shan, D. E. Shaw, "Scalable

Algorithms for Molecular Dynamics Simulations on Commodity Clusters" in *SC '06: Proceedings of the 2006 ACM/IEEE Conference on Supercomputing* (2006), pp. 43–43.
73. S. Nosé, A unified formulation of the constant temperature molecular dynamics methods. *J. Chem. Phys.* **81**, 511–519 (1984).
74. Z. Deng, C. Chuaqui, J. Singh, Structural interaction fingerprint (SIFt): A novel method for analyzing three-dimensional protein-ligand binding interactions. *J. Med. Chem.* **47**, 337–344 (2004).
75. F. Noé, C. Schütte, E. Vanden-Eijnden, L. Reich, T. R. Weikl, Constructing the equilibrium ensemble of folding pathways from short off-equilibrium simulations. *Proc. Natl. Acad. Sci. U.S.A.* **106**, 19011–19016 (2009).
76. C. E. Shannon, A mathematical theory of communication. *Bell Syst. Tech. J.* **27**, 379–423 (1948).
77. C. X. Hernández, V. S. Pande, MDEntropy: Information-theoretic analyses for molecular dynamics. *J. Open Source Softw.* **2**, 427 (2017).
78. A. Hagberg, P. J. Swart, D. A. Schult, "Exploring network structure, dynamics, and function using NetworkX" (LA-UR-08-05495; LA-UR-08-5495, Los Alamos National Laboratory (LANL), Los Alamos, NM (United States), 2008); https://osti.gov/biblio/960616.

Acknowledgments: We would like to acknowledge the support of the structural work by members of the National Center for cryo-EM Access and Training (NCCAT) and the Simons Electron Microscopy Center located at the New York Structural Biology Center, supported by the NIH Common Fund Transformative High Resolution Cryo-Electron Microscopy program (U24 GM129539,) and by grants from the Simons Foundation (SF349247) and NY State Assembly. We further acknowledge the staff at the Laboratory for BioMolecular Structure (LBMS), which is supported by the DOE Office of Biological and Environmental Research (KP160711). This work was supported in part through the computational resources and staff expertise provided by Scientific Computing at the Icahn School of Medicine at Mount Sinai and supported by the Clinical and Translational Science Awards (CTSA) grant UL1TR004419 from the National Center for Advancing Translational Sciences. We would also like to acknowledge J. McCorvy for critical evaluation of the manuscript. **Funding:** This work was supported by NIH grant GM133504, a Sloan Research Fellowship in Neuroscience, an Edward Mallinckrodt, Jr. Foundation Grant, and a McKnight Foundation Scholars Award (all to D.W.). Further support came from NIH T32 Training grants GM062754 and DA053558 (G.Z. and A.L.W.) and NIH F31 fellowship MH132317 (A.L.W.). **Author contributions:** Conceptualization: G.Z., A.K.P., A.L.W., B.F., D.P., M.F., and D.W. Methodology: G.Z., A.K.P., A.L.W., B.F., D.P., M.F., and D.W. Investigation: G.Z., A.K.P., A.L.W., and B.F. Visualization: G.Z., A.K.P., A.L.W., B.F., and D.W. Supervision: A.L.W., M.F., and D.W. Writing—original draft: G.Z., A.K.P., A.L.W., and D.W. Writing—review and editing: G.Z., A.K.P., A.L.W., B.F., D.P., M.F., and D.W. Resources: A.K.P., B.F., D.W., and D.P. Data curation: A.K.P., A.L.W., and D.P. Validation: GZ.,. A.K.P., A.L.W., B.F., and D.W. Formal analysis: G.Z., A.K.P., A.L.W., B.F., D.P., and D.W. Project administration: A.K.P., A.L.W., D.P., M.F., and D.W. Funding acquisition: D.W. **Competing interests:** The authors declare that they have no competing interests. **Data and materials availability:** All data needed to evaluate the conclusions in the paper are present in the paper and/or the Supplementary Materials. Density maps and structure coordinates have been deposited in the Electron Microscopy Data Bank (EMDB) and the PDB: mianserin/5-HT_{1e}R–Gα_{i1}–Gβ_1–Gγ_2 (EMD-42241 and PDB 8UGY) and setiptiline/5-HT_{1e}R–Gα_{i1}–Gβ_1–Gγ_2/scFV16 (EMD-42245 and PDB 8UH3). Correspondence and requests for materials should be addressed to daniel.wacker@mssm.edu.

Submitted 5 October 2023
Accepted 15 March 2024
Published 17 April 2024
10.1126/sciadv.adk4855